A 22 GHz RADIO TELESCOPE

A thesis submitted for the degree of Master of Science

at Rhodes University, Grahamstown

by

LAURENCE IAN MUTCH

Supervisors: Prof. E.E. Baart

Dr. G. de Jager

July 1975

ACKNOWLEDGEMENTS

Our Radio Astronomy research project and the work covered in this thesis is the result of the efforts of many. The Radio Astronomy Group is under the direction of Professor E. E. Baart, Dr. G. de Jager and Clive Way-Jones. My sincere appreciation to them for an enormous amount of advice and assistance.

I would like to extend a special vote of thanks to Dr. Jacob W. M. Baars for a guiding hand to us all during his visit in March and April, 1975.

Brian Nunn (1974) designed the Cassegrain and Front End supports and with Clive Way-Jones designed and built sections of the Control Logic and Data Capture Systems.

Mike Gaylard is responsible for the Front End layout and alignment of the telescope and has assisted in receiver construction and testing.

Graham Oberem is developing the telescope position feedback network.

Jörg Lichtenberg is a very capable man and his efforts are many and varied from the construction of the Front End power supplies to the design and construction of the U. T. and Sidereal Time clocks and motor drive system.

Ron Arnott, Angus Barnard, Owen Campbell, Del Gillam, Georg Gruber and Mike Inggs - all gave many hours and the system is a tribute to their efforts.

My final thanks go to Pete Mountfort, our Computer Systems expert, for a great deal of assistance and discussion and to Bev Taylor for skilfully typing this work.

Laurie Mutch

CONTENTS

ABSTRACT

This thesis reports on the design, construction, testing and operation of the spectral line and continuum receivers built for the 22 GHz Radio Telescope. First results from the telescope were obtained and have been analysed to give an estimate of system efficiency. Tests have been performed on the front end and in particular on the 22 GHz mixer in order to determine the minimum detectable temperature. The Sun, Moon and major planets are sources suitable for antenna alignment and consequently a literature survey of emission at 22 GHz from elements of the Solar system has been made.

PREFACE

The high frequency unit, known as the Front End, is studied first in Chapter One. This is followed in Chapter Two with a description of the design, construction and operation of the spectral line and continuum receivers. Chapters Three and Four deal, in turn, with the procedures adopted in tracking a radio source and with tests performed on a paint surface applied to the main parabolic dish of the telescope. A literature survey of 22 GHz emission from elements of the Solar system is presented in Chapter Five. Finally Chapter Six reports on first results from the telescope and gives estimates of the system efficiency.

CHAPTER ONE

THE FRONT END

CHAPTER ONE

THE FRONT END

The sections of the 22 GHz Radio Telescope completed or under construction at this stage are depicted in Figure 1. 1. This chapter reports on the front end or high frequency unit.

1. 1 Before the mixer

The Cassegrain design of the telescope allows the front end to be mounted on a base plate immediately behind the main reflector. Figure 1. 2 illustrates the front end alternatives depending upon which receiver is in operation. The effect of gain variations can be reduced if the receiver input is continuously switched between the signal from the main antenna horn and a reference signal.

In the continuum or total power configuration the reference signal is provided via a secondary horn pointing off axis at another part of the sky. By means of phase sensitive rectification (see Section 2. 5) receiver instabilities and sky noise may be subtracted out. A 22 GHz noise source signal may be added to the main beam for calibration purposes by means of a variable attenuator and a 20 dB cross coupler.

In the spectral line system frequency switching (see Section 1. 3) is used and hence the input is fed directly to the mixer by holding the microwave switch open in this line. The reference horn is not used.

In an alternative spectral line arrangement (Option B, Figure 1. 2) the microwave switch is used to synchronously switch the reference noise source in and out of the system via an attenuator and a 20 dB directional coupler. The microwave switch has an insertion loss of approximately

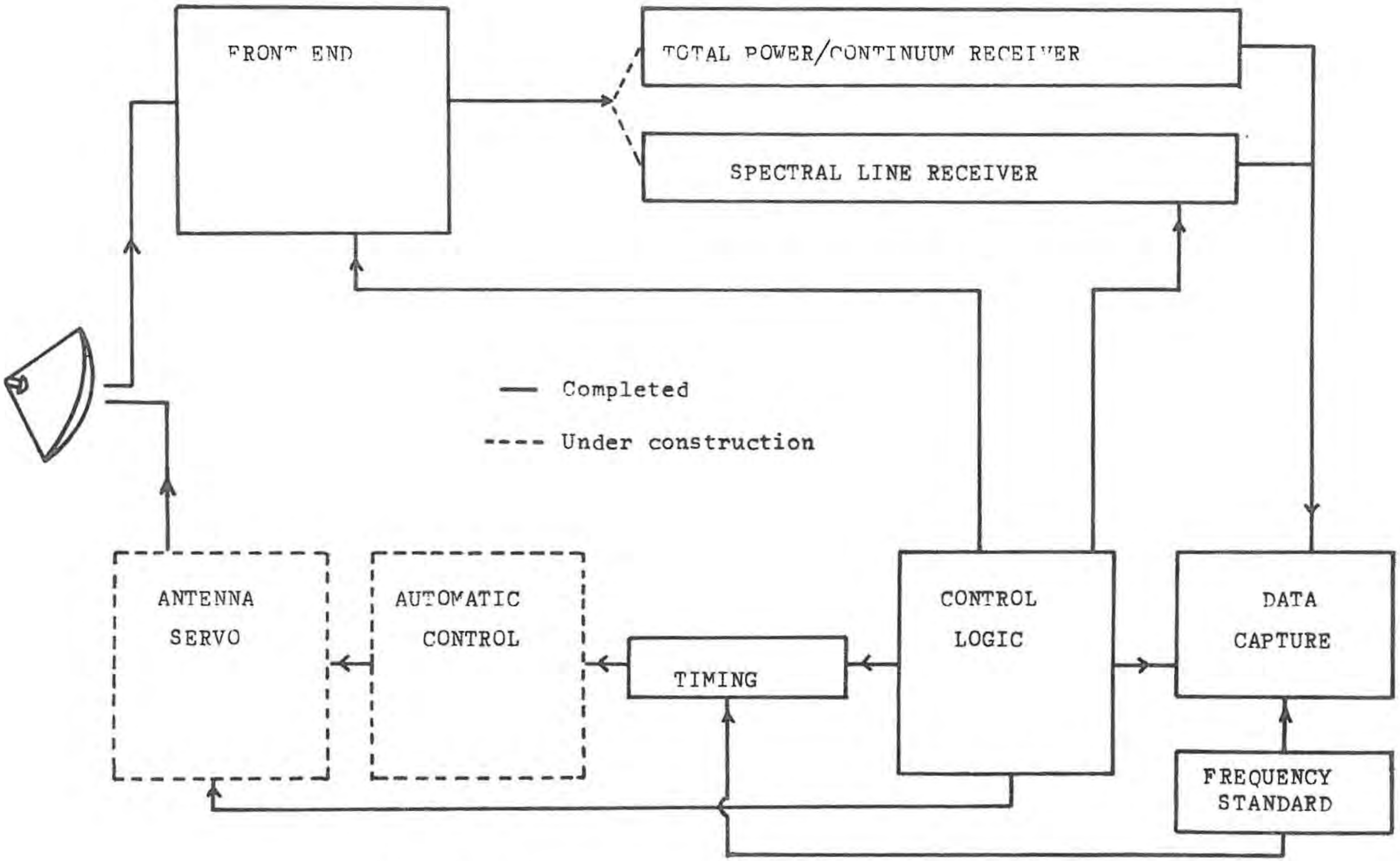

FIGURE 1.1

SCHEMATIC - RADIO TELESCOPE

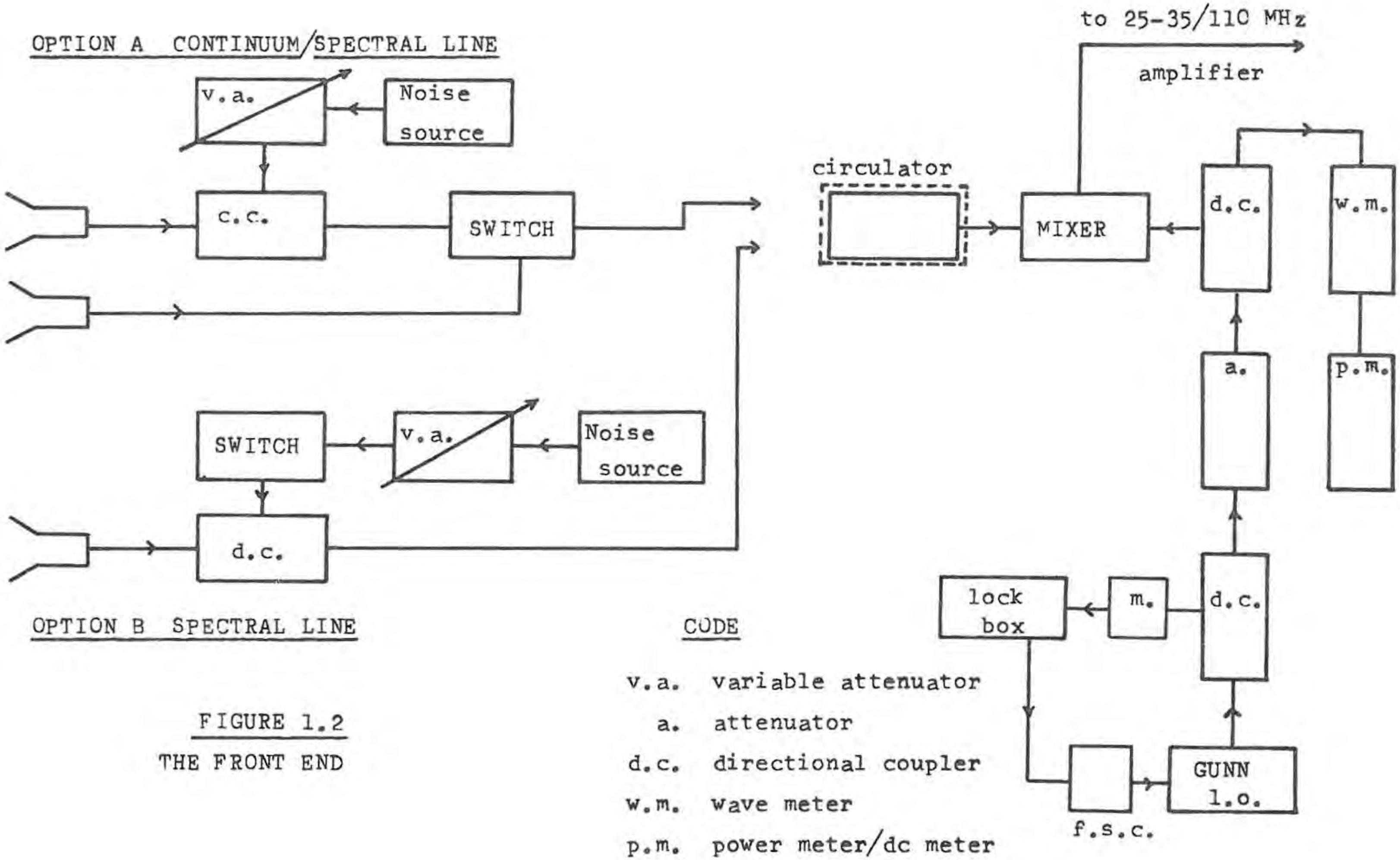

FIGURE 1.2
THE FRONT END

CODE

v.a.	variable attenuator
a.	attenuator
d.c.	directional coupler
w.m.	wave meter
p.m.	power meter/dc meter
l.o.	local oscillator
c.c.	cross coupler
m.	mixer
f.s.c.	frequency switch circuit

0, 3 dB and its removal from the waveguide between the horn and the mixer effectively reduces the attenuation before the mixer. The manufacturer's specifications of major front end components are given in Appendix A1.

The noise source

The noise source is an argon filled gas discharge tube type BS 386 made by English Electric Valve Company. This is mounted in a holder, MC 20/32A, made by Mid-Century Microwavegear. Data for this mount type shows the excess noise ratio (ENR) to be 15, 93 dB but specifies a tube type, TD 13, made by Signalite Inc. This anomaly has resulted in some doubt as to the true ENR of the noise source. English Electric estimate that the ENR for tube BS 382 (presumably similar to BS 386) in an MC 20/32A is 16, 2 dB at 22 GHz. All future calibrations are based on an ENR of 16, 07 dB, the mean of these two estimates. The uncertainty in this figure is approximately 3%.

$$\mathrm{ENR} = (T_G - T_0)/T_0 = 16,07\ \mathrm{dB} \qquad 1.1$$

Therefore the noise source temperature,

$$\underline{T_G = 12000 \pm 400\ \mathrm{K}} \quad \text{if } T_0 = 290\ \mathrm{K}$$

Baars (1975) has suggested that this uncertainty in ENR could be resolved by calibrating the receiver system using a "hot-cold-load" method.

This type of gas noise tube requires a striking voltage of 3, 1 kV. The pulse starts the discharge which is then sustained by a power supply voltage of between 65 and 165 volts. Rapid switching of the noise tube by switching the power supply is not possible and hence a ferrite circulator — is used.

The switch

The microwave switch is a latching ferrite circulator with a transistor-transistor-logic (TTL) driver. It acts as a non reciprocal latching single pole-double throw switch that transmits microwave energy with low insertion loss ($\leqslant$ 0, 3 dB) between ports in a clockwise direction for one switched state and in an anticlockwise direction for the opposite switched state. High isolation ($\geqslant$ 20 dB) is maintained between open and closed ports. The switch is designed to operate between 21, 6 and 22, 8 GHz.

Fast switching is desirable in order that the receiver gain change in one cycle is small and hence this type of microwave switching is performed by modulating ferrite devices with an electromagnet. The switching energy is 270 microjoules and the switching speed is limited to 100 microseconds because of demagnetizing fields determined by the shape of the ferrite and because of eddy currents induced in the waveguide walls due to the changing magnetic field (Helszajn, 1969, page 245).

The microwave switch is controlled by the circuit shown in Appendix A2. This circuit receives an input switch signal from the receiver control unit in the main rack. Switching occurs when either trigger line receives a transition from the logical "0" to "1" state. Provision has been made for a second TTL circulator or switch as illustrated in Figure 1. 2 (dotted lines). The circuit provides switching in a clockwise or anti-clockwise direction and allows either input port to be maintained in an open position. This is necessary for spectral line applications when frequency switching the local oscillator. The circuit also provides a frequency switch signal buffer (see Frequency switching, Section 1. 3). A requirement of this second form of switching is that the local oscillator is phase locked whilst on the spectral line frequency.

1.2 The local oscillator and phase locking

The local oscillator

The high-frequency, local oscillator signal in the front end is provided by a Gunn-effect oscillator. Two of the Gunns used, made by Varian, have electronic as well as coarse mechanical tuning and are thus suitable for phase locking. The third Gunn, manufactured by Mid-Century Microwavegear has accurate mechanical tuning only.

In the case of electronically tunable oscillators the device is mechanically tuned by varying the sliding short circuit position and the frequency of oscillation corresponds to a half-wavelength of the cavity length. High speed electronic tuning about the frequency set by the mechanical tuning is possible by using varactor diodes.

Phase locking

Stabilization of the local oscillator signal is necessary for spectral line measurements. This is provided by a Sage model 251 B microwave oscillator synchronizer.

The synchronizer samples the oscillator output and mixes the sample with a "comb" of harmonic lines, 100 MHz apart, derived from a crystal reference oscillator, to obtain a 25 MHz intermediate beat frequency. The synchronizer then phase compares this 25 MHz IF signal with a 25 MHz reference signal derived by carefully multiplying the same crystal reference. When there is a phase difference, the comparator generates an error voltage which is applied to the varactor diode in the oscillator to correct the difference. Hence, when the oscillator drifts a phase error is detected and a correcting voltage is applied.

The RF reference frequency is generated by one of ten crystal oscillators centred about 5 MHz which are temperature stabilized in an oven. There is also a nine position phase lag unit in the feedback circuit which allows for optimum noise reduction by optimizing loop stability. The unit essentially allows the selection of one of nine lead-lag networks.

The frequency of the spectral line varies as a consequence of the relative motion of the source and the Earth. This motion determines the choice of local oscillator frequency and the local oscillator frequency establishes which of the ten crystals may be used for phase locking.

Table 1.1 presents the Sage crystal frequencies, tuning ranges and suitable harmonics of the frequencies plus or minus the 25 MHz intermediate beat frequency. Only frequencies within the tuning range of the Varian Gunn oscillators (22180 - 22330 MHz) have been calculated. The harmonics are 100 MHz apart and hence only every 20th harmonic of the 5 MHz crystal is selected. The harmonics are shown graphically in Figure 1.3. There is a gap of approximately 20 MHz between the harmonic minus the IF and the harmonic plus the IF. Clearly the Gunn will not lock onto that crystal in the gap. For example, if the Gunn is tuned to 22, 265 GHz it may be locked to the 4440th harmonic of crystal 7, 9 or 10 but not 8.

1.3 Frequency switching

In the case of spectral line measurements the range of frequencies of interest is very narrow in contrast to the broad base line formed by the atmospheric line profile. The effect of receiver instabilities is reduced by frequency switching the front end local oscillator on and off the spectral line frequency by adjusting the voltage applied to the varactor. As mentioned in Section 1.2 stabilization of the local oscillator signal is essential for spectral line studies and thus the oscillator must be locked whilst in the

TABLE 1.1

Harmonics of Crystal frequencies within range of Varian Gunns

(22180 - 22330 MHz)

Crystal	Range (MHz)		Crystal Range x 4420th Harmonic	-25 MHz	+25 MHz
8	5,0104	5,01675	22146 - 22174		22171 - 22199
9	5,01441	5,0217	22164 - 22196		22188 - 22221
10	5,01948	5,02674	22186 - 22218	22161 - 22193	22211 - 22243
			x 4440		
3	4,98537	4,99187	22135 - 22164		22160 - 22189
4	4,98948	4,99685	22153 - 22186		22178 - 22211
5	4,9946	5,00172	22176 - 22208	22151 - 22183	22201 - 22233
6	5,00079	5,00676	22204 - 22230	22179 - 22205	22229 - 22255
7	5,00316	5,0116	22214 - 22251	22189 - 22226	22239 - 22276
8	5,0104	5,01675	22246 - 22274	22221 - 22249	22271 - 22299
9	5,01441	5,0217	22264 - 22296	22239 - 22271	22289 - 22321
10	5,01948	5,02674	22286 - 22319	22261 - 22294	22311 - 22344
			x 4460		
1	4,9756	4,98187	22191 - 22219	22166 - 22194	22216 - 22244
2	4,98041	4,98684	22213 - 22241	22188 - 22216	22238 - 22266
3	4,98537	4,99187	22235 - 22264	22210 - 22239	22260 - 22289
4	4,98948	4,99685	22253 - 22286	22228 - 22261	22278 - 22311
5	4,9946	5,00172	22276 - 22308	22251 - 22283	22301 - 22333
6	5,00079	5,00676	22304 - 22330	22279 - 22305	22329 - 22355
7	5,00316	5,0116	22314 - 22352	22289 - 22327	
8	5,0104	5,01675	22346 - 22375	22321 - 22350	
			x 4480		
1	4,9756	4,98187	22291 - 22319	22266 - 22294	22316 - 22344
2	4,98041	4,98684	22312 - 22341	22287 - 22316	
3	4,98537	4,99187	22334 - 22364	22309 - 22339	
4	4,98948	4,99685	22352 - 22386	22327 - 22361	

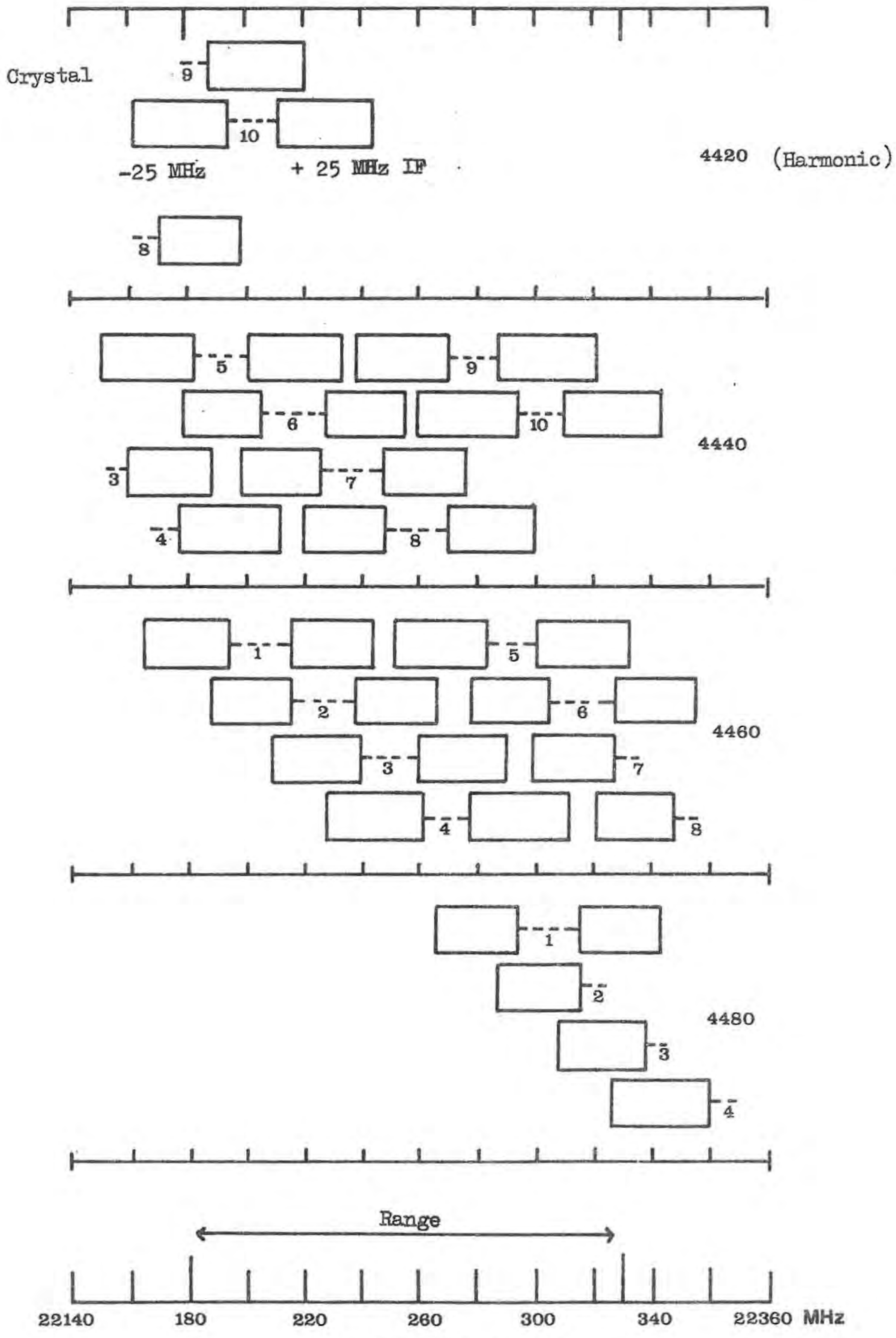

FIGURE 1.3

HARMONICS OF SAGE CRYSTAL FREQUENCIES WITHIN RANGE OF VARIAN GUNNS. (22180 - 22330 MHz) "on" state. The lock acquisition time must be small when compared with the "on" half-cycle. For maximum efficiency the time taken to phase lock the local oscillator onto the spectral line must be minimal. The acquisition time determines the switch rate and hence the design of filters in the receiver channels. Figure 1.4 illustrates a trial circuit which was built to test the feasibility of frequency switching the Varian Gunns. The purpose of this circuit is to apply a square wave switch signal to the Gunn varactor.

A switch signal of variable amplitude from the frequency switch signal buffer in the microwave switch control circuit (see Appendix A2) is added, by using an LM 3900 operational amplifier, to a variable dc offset generated from the circuit in the bottom right of Figure 1.4 and the attenuated error voltage from the Sage synchronizer and applied to the varactor. A diode protection circuit is provided to ensure the oscillator does not receive a negative voltage spike.

The Gunn was initially tuned mechanically and by means of the dc offset to a predetermined local oscillator frequency, for example, 22,255 GHz. A particular Sage crystal and the amplitude of the switch signal are chosen such that the Gunn frequency in the "off" state will be above or below the locking range of the crystal. The local oscillator will not lock reliably both on and off the spectral line and hence the Gunn is locked during the "on" state and then allowed to drift in a different frequency region during the "off" state. The frequency switch circuit gives a varactor modulation sensitivity of approximately 6,5 MHz per volt and hence a 2,6 volt swing from 8,4 to 11,0 volts will switch the oscillator from 22,255 GHz to 22,273 GHz. The Gunn was locked to crystal 7 of the Sage (see Figure 1.3) in the "on" state. The mode switch (lag network, see Section 1.2) was adjusted to correspond to

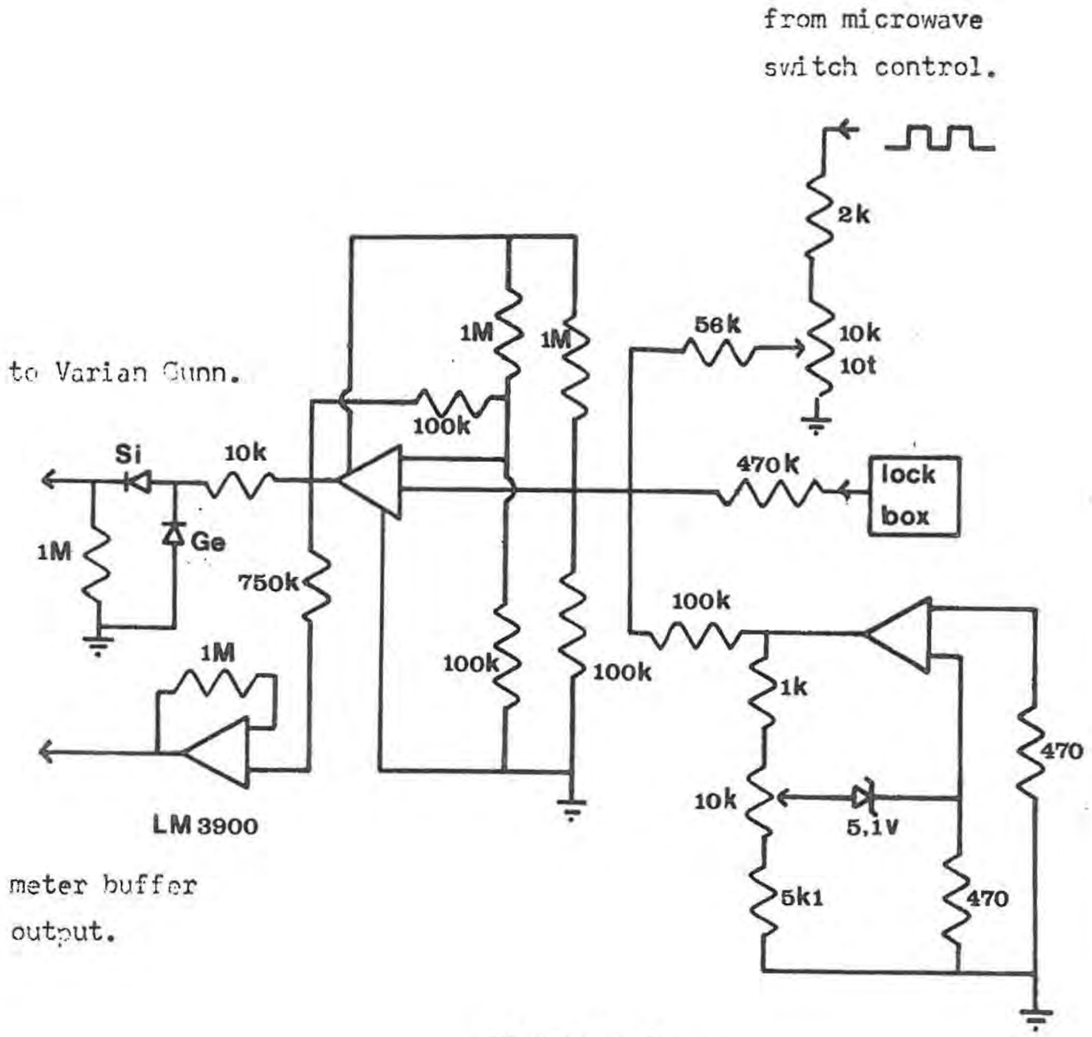

FIGURE 1.4
FREQUENCY SWITCH CIRCUIT.

the modulation sensitivity (position 3 for 4 to 8 MHz per volt).

Figure 1.5 indicates the output of the synchronizer phase detector and lock light indicator as observed during the test described above. The signals at these two outputs indicate when the "locked" state has been reached. The period of transition between the "out of lock" state and the "locked" state has been expanded by using a time-base delay on a monitor oscilloscope. The expanded outputs are compared in time with the voltage applied to the varactor in the Gunn oscillator. The synchronizer applies a down pulse to the Gunn varactor as the 11,0 voltage level is switched. The 8,4 voltage level is reached after approximately 35 microseconds. The synchronizer then initiates a search which corresponds to the vertical lines from -400 mV to +400 mV in the phase detector output. The lock acquisition time, T, is the time taken to reach the "locked" state after the 8,4 voltage level applied to the varactor has been attained. The measured acquisition time was 60 microseconds. A switching frequency of the order of 100 Hz may thus be used because the acquisition time is then about 1% of a half-cycle. The output of the phase detector should be studied in order to measure acquisition time rather than the lock light indicator output because of the response delay of the light indicator as shown in Figure 1.5.

A very similar technique to that described above was adopted by Nicholson (1974) at 100 GHz. The topic of lock acquisition is discussed by Gardner (1966), page 40.

1.4 Front end power levels

The manufacturer's specifications (see Appendix A1) indicate that the Sage mixer requires an RF input from -30 dBm to 0 dBm. The Varian Gunns generate between 52 and 64 mW of power, hence a 20 dB directional

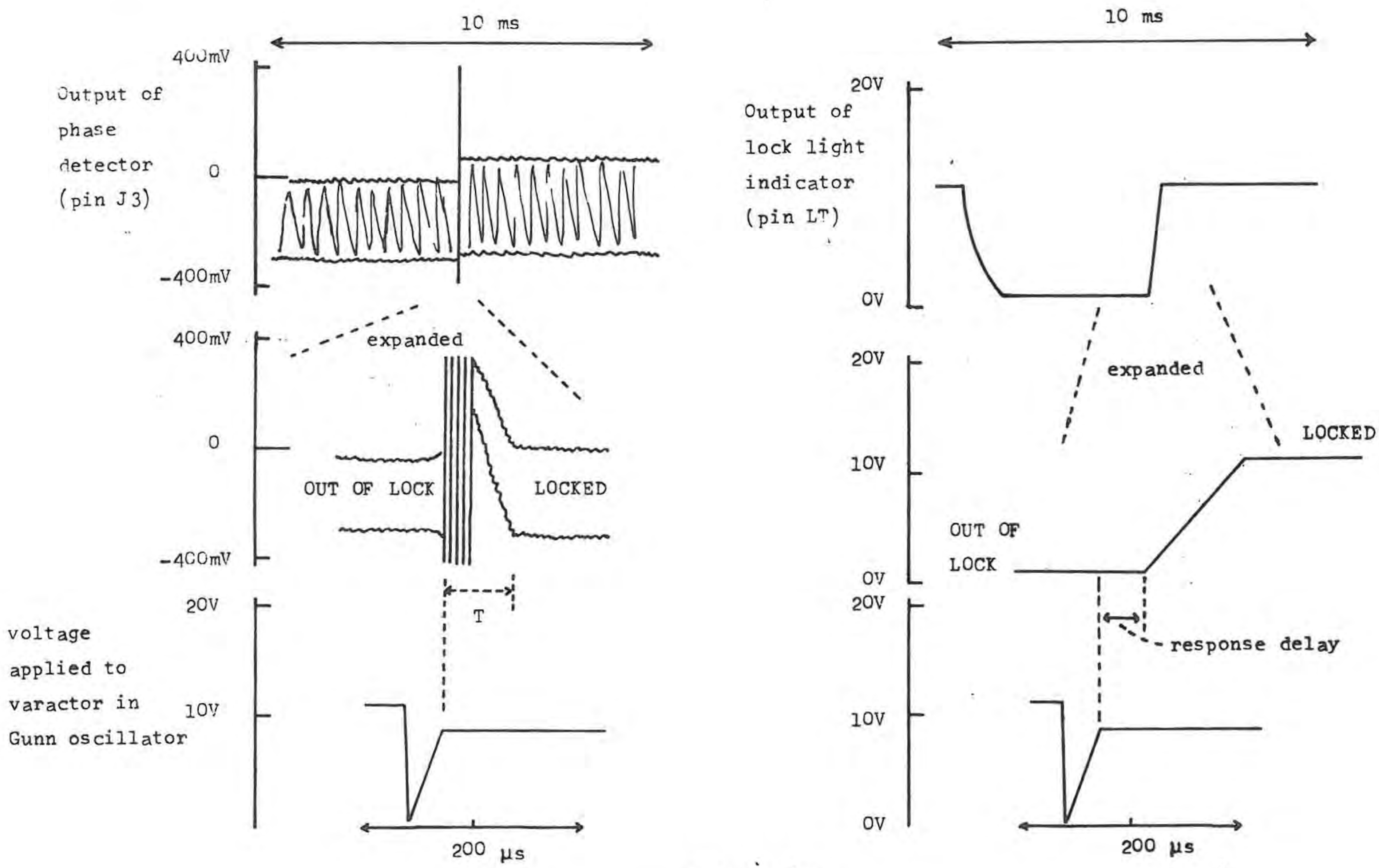

FIGURE 1.5

SAGE SYNCHRONIZER PHASE DETECTOR AND LOCK LIGHT INDICATOR OUTPUT coupler is used to connect the local oscillator to the Sage synchronizer mixer. This provides an RF input of between -2,84 and -1,94 dBm.

The maximum local oscillator input to the Aerojet mixer is 2 mW (see Section 1.5). Hence a minimum of 15,05 dB of attenuation is required before the mixer input port.

Provision has been made in the front-end arrangement for a Hewlett-Packard power meter to be used with the frequency wavemeter (see Figure 1.2). The H-P thermistor mount is limited to 15 mW input and the power meter scale to 10 mW. Hence at least 8,1 dB of attenuation must be between the local oscillator and power meter mount.

1.5 The mixer

The double-ended microwave mixer is used in superheterodyne receivers to balance out local oscillator amplitude modulated noise at the input to the IF amplifier in the mixer whilst deriving a difference signal.

Two Schottky (hot carrier) diodes are used. These have a metal-semiconductor interface which exhibits a non-linear impedance. The diodes are located at the two ends of the through arm of a magic-T. The local oscillator signal is fed into the H-plane arm and will arrive at the diodes in phase. The signal is fed into the E-plane arm and will arrive at the two diodes out of phase. The difference frequency (IF) signal produced by mixing in the non-linear diodes will be 180^{o} out of phase, but the local oscillator noise will be in phase at the diodes. If the diode outputs are fed into a push-pull balanced IF input the noise will cancel but the IF signals add up in phase.

An important advantage obtained with the use of a magic-T arrangement is the prevention of radiation by the local oscillator. The E and H planes are uncoupled so that the local oscillator signal cannot be coupled to the antenna (Collin, 1966, page 286).

The Aerojet K-band mixer layout is shown in Figure 1.6. The transition from waveguide to microstrip takes place by means of a ridged transducer. This transforms the input waveguide impedance to that of the microstrip (Araki, 1971). The transistors are used to give constant bias current.

The diode currents may be monitored between the -i and -15 V pins and between the +i and +15 V pins. Early testing of the mixer indicated that the negative diode was damaged (see Table 1.2). The spare matched diodes supplied were installed. Elder (1969), page 375, reports that the diodes must be handled carefully to avoid damage resulting from accidental electrostatic discharge. Araki (1971) subjected a 22 GHz mixer to very severe shock tests and reports excellent reliability.

Table 1.2

Diode current monitoring

	Manufacturer's measurements	Damaged diodes	Replacement diodes
Bias only	+150 μA	+150 μA	+130 μA
	- 30 μA	- 1,00 mA	- 48 μA
L.O. + bias	+1,12 mA	+ 1,10 mA	+ 1,00 mA
	-1,05 mA	-1,00 mA	- 1,20 mA

The IF amplifier in the mixer mount has been tested using a spectrum analyser. A gain of 37 dB was measured from 10 to 114,9 MHz. This is in agreement with the manufacturer's specifications (see Appendix A1).

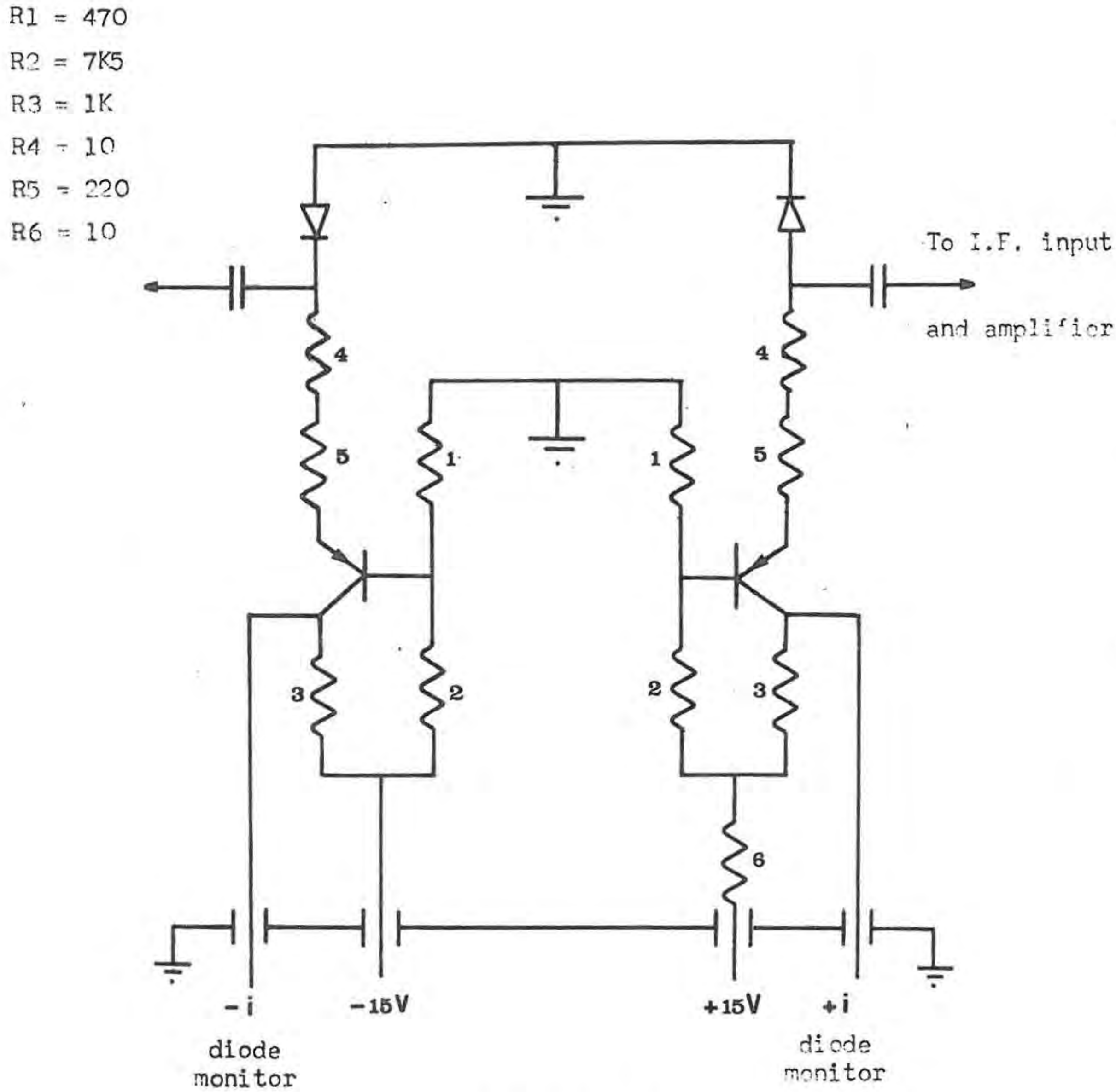

FIGURE 1.6
AEROJET K-BAND MIXER LAYOUT

Noise temperature

The noise figure for the mixer was measured using both the Y-factor and 3 dB methods at various local oscillator power levels with the test layout shown in Figure 1. 7.

FIGURE 1.7

MIXER NOISE FIGURE
TEST ARRANGEMENT.

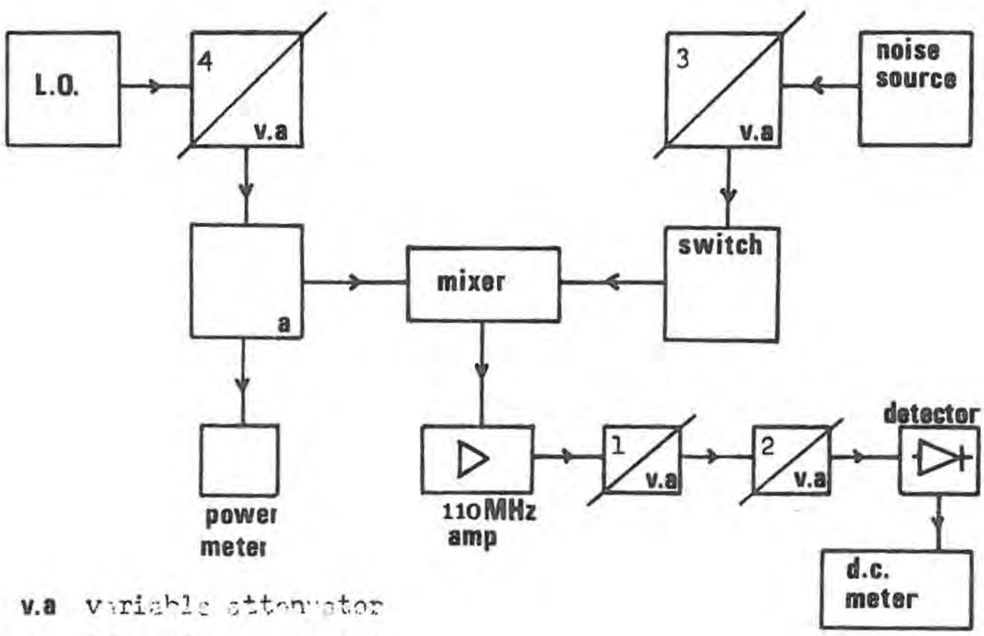

v.a variable attenuator
a 10,5 dB attenuator.

a) Y-factor method

A reference detector level is set using variable attenuators 1 and 2 with the noise source off. The noise generator is then fired and this results in a higher detector reading. Attenuators 1 and 2 are then carefully re-adjusted to give the original reference level. The change in attenuator level is the Y-factor. The noise figure, F, of the mixer is given by: (Microwave Engineers' Handbook Vol.2, 1971, page 122; Kraus, 1966, page 286).

$$F(dB) = 10 \log (T_C/T_0 - 1) - 10 \log (Y_\ell - 1) \qquad 1.2$$

where

$$T_C = (T_G - T_0)/L + T_0 \qquad 1.3$$

T_G = noise source temperature = 12000 $\pm$400 K (see Section 1. 1)

L = linear attenuation between the noise generator and the mixer

T_0 = 290 K

Y (dB) = 10 log Y_ℓ

F (dB) = 10 log F_ℓ

The waveguide and joins between the noise tube and mixer contribute about 0, 1 dB and the insertion loss of the switch is about 0, 3 dB resulting in an additional 0, 4 dB of attenuation. This contribution must be taken into account in the determination of L.

The noise figure measurements obtained using this method for several settings of attenuator 3 (noise source attenuation) and a range of local oscillator levels are shown in Figure 1. 8. Three important results may be deduced.

1) The minimum mixer noise figure (Y-factor maximum) for a particular noise source level occurs between local oscillator levels of 0, 2 and 0, 3 mW. This is in agreement with the results for receivers at the Effelsberg telescope at Bonn (de Jager, 1975). The manufacturer's specifications for the mixer quote a figure of 2 mW for the local oscillator input. It is thought that this refers to maximum input rather than optimum input.

2) The measured mixer noise figure improves with decreasing input from the noise source. Kraus (1966), page 287, warns that the noise

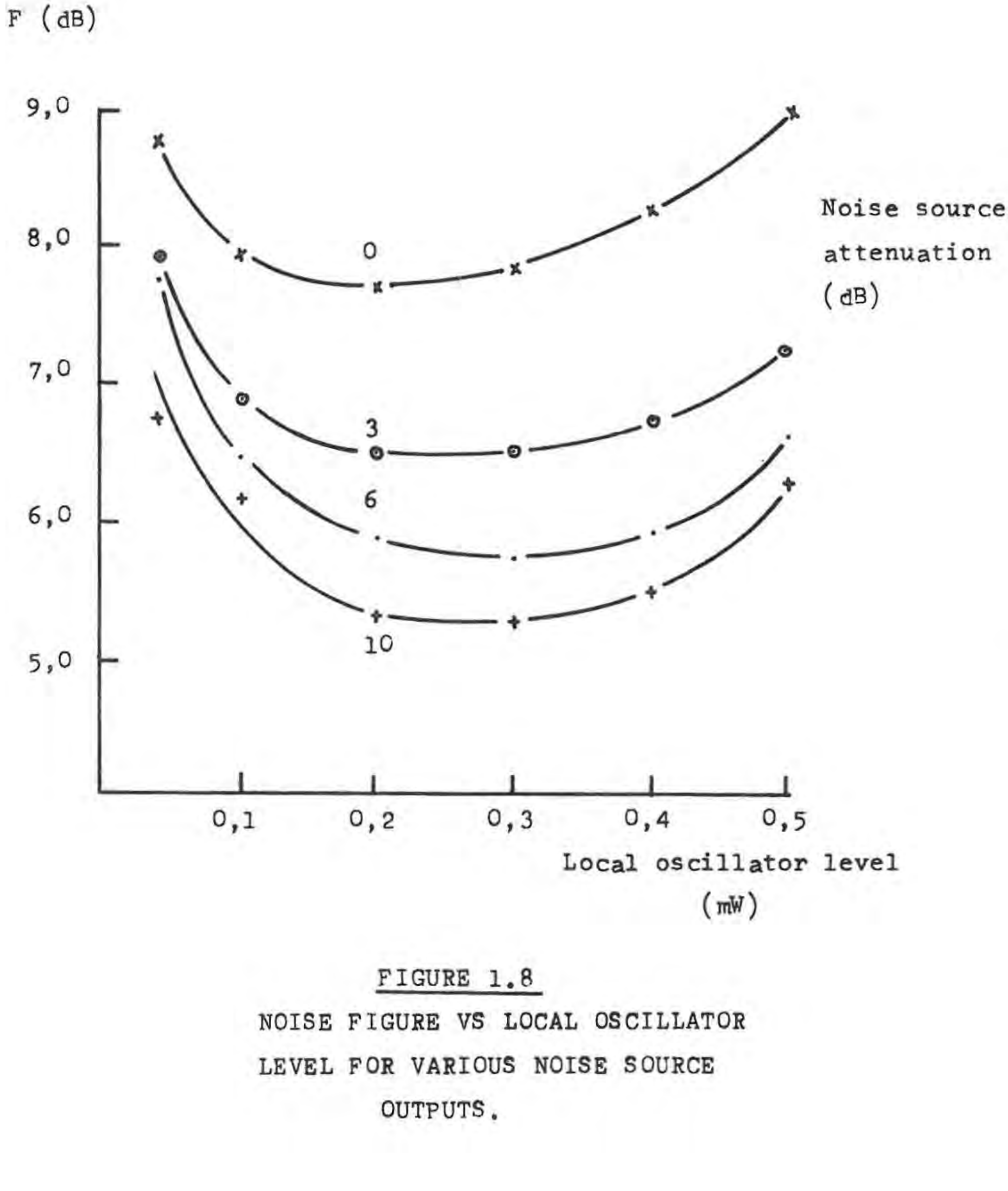

FIGURE 1.8

NOISE FIGURE VS LOCAL OSCILLATOR LEVEL FOR VARIOUS NOISE SOURCE OUTPUTS.

input, T_C, should be of the same order of magnitude as the mixer noise temperature, T_R. A substantially larger noise input will result in an erroneous figure for T_R. The mixer noise temperature includes noise attributable to the IF amplifier in the mixer mount and may be considered the receiver noise temperature.

$$T_R = (F_\ell - 1)\, T_0 \qquad 1.4$$

3) The minimum mixer noise temperature may be calculated from a noise figure, F, of 5,3 dB (Y-factor of 3,2 dB) at 0,3 mW with variable attenuator 3 set at 10 dB. The attenuators used in these measurements have been tested. Attenuators 1 and 2, manufactured by Alan Industries are accurate to at least 0,1 dB. The measured calibration curve of attenuator 3, manufactured by Mid-Century Microwavegear, differs from the manufacturer's specifications by 0,4 dB at 10 dB. Attenuator 4, manufactured by Mid-Century, differs by 0,1 dB at 22,6 dB, the attenuation required to reduce the local oscillator level to 0,3 mW.

$Y = 3{,}2 \pm 0{,}1$ dB

$L = 10{,}4 \pm 0{,}4$ dB

$F = 5{,}3 \pm 0{,}5$ dB (from eqn. 1.2)

$F_\ell = 3{,}4 \pm 0{,}4$

Therefore $\underline{T_R = 700 \pm 100 \text{ K}}$ (from eqn 1.4)

b) <u>3 dB method</u>

The reference detector level is noted with the noise tube off. The dc meter reading is related to the power, W, out of the mixer and amplifier such that:

$$W = G\,k\,T\,B \qquad 1.5$$

where

G = amplifier gain

B = bandwidth

k = Boltzmann's constant

$T = T_R + T_0$

Attenuators 1 and 2 are then carefully adjusted to provide an additional 3 dB of attenuation. Nearly twice the original output is then required to reach the reference level. The noise tube is fired and attenuator 3 is adjusted to give the same reference level as before

The procedure may be presented as follows:

1) Noise tube unfired ; reference level related to

$$W = Gk\ (T_0 + T_R)\ B$$

2) 3 dB inserted

3) Noise tube fired ; $W' = Gk\ (T_C + T_R)\ B$

Therefore $$2\ (T_0 + T_R) = T_C + T_R$$

$$T_R = T_C - 2\ T_0 \qquad 1.6$$

where $$T_C = (T_G - T_0)/L + T_0$$

(from eqn. 1.3)

As in the Y-factor method the procedure was repeated for a range of local oscillator levels. The maximum setting of attenuator 3 (11, 3 dB), corresponding to a minimum noise figure was obtained at a local oscillator level of 0, 25 mW in agreement with the Y-factor measurements. The uncertainty in attenuator 3 is again 0, 4 dB.

Hence $L = 11,3 + 0,4 \pm 0,4$ dB

$T_C = 1100 \pm 100$ K (from eqn 1. 3)

$\underline{T_R = 500 \pm 100 \text{ K}}$ (from eqn 1.6)

The mean mixer noise temperature from these two methods is 600 ± 100 K at 0, 25 mW local oscillator input. This result may be compared with measurements made by Aerojet. They claim:

$F = 4,4$ dB at 22 GHz

Hence $T_R = 509$ K

In Section 1.4 a minimum attenuation of 15,05 dB between the local oscillator and mixer input was quoted. This figure is calculated on a maximum of 2 mW input. The results above indicate that for minimum mixer noise 0,25 mW input is required which corresponds to between 23 dB and 24 dB attenuation depending upon which Varian Gunn is used.

The noise temperatures above are the double channel figures for the mixer. For continuum measurements both signal and image channels can be used. The spectral line noise temperature is almost twice the double channel figure.

1.6 Minimum detectable temperature

The measurement of the mixer noise temperature enables an estimate to be made of the system temperature, T_{sys}, and hence the minimum detectable temperature, ΔT_{min}. From Kraus (1966), page 240:

$$T_{sys} = T_A + T_{RT}$$

where

T_A = antenna temperature

$T_{RT} = (L - 1)\, T_0 + L\, T_R$

L = attenuation in transmission line and switch

= 0,4 dB

The antenna temperature, T_A, arises mostly from radiation by the atmosphere (about 50 K). Kraus (1966), page 102, presents the minimum detectable temperature as:

$$\Delta T_{min} = K_s \; T_{sys} / (\Delta\nu \, t \, n)^{\frac{1}{2}}$$

where

K_s = sensitivity constant of receiver = 2

$\Delta\nu$ = predetection bandwidth

t = postdetection integration time

n = number of records included

The figures for our two alternative systems are then

	Spectral line	Continuum
T_R	1200 K	600 K
T_{sys} (option A, Figure 1.2)	1400 K	740 K
$\Delta\nu$	50 kHz	100 MHz
ΔT_{min}	$12,5 \pm 1,8/(tn)^{\frac{1}{2}}$K	$0,15 \pm 0,02/(tn)^{\frac{1}{2}}$K

The significance of these results will be clear at the conclusion of Chapter Five.

CHAPTER TWO

THE SPECTRAL LINE AND CONTINUUM RECEIVERS

CHAPTER TWO

THE SPECTRAL LINE AND CONTINUUM RECEIVERS

A The spectral line receiver

The spectral line receiver was designed on the basis of resolution and cost. The sources of interest typically exhibit Doppler-shifted peaks of emission corresponding to velocity differences as small as 2/3 kilometre per second. The peaks are generally spread over a 20-kilometre-per-second range of radial velocity relative to the mean local standard of rest (Johnston et al., 1972). These factors have determined the number of channels required. Fifty 50 kHz channels resulting in a resolution of 0, 7 kilometre per second within a range of 34 kilometres per second are being built. This number of channels will eventually be extended to one hundred.

The multichannel receiver is housed in the main rack with the continuum receiver (see Section B), receiver logic, telescope drive control, position readout systems and receiver and logic power supplies (see Section C and Appendix B4).

The radio telescope was initially developed to observe the $6_{16} \rightarrow 5_{23}$ microwave transition of water vapour at 22, 23508 GHz (1, 348 cm wavelength) discovered by Cheung et al. (1969) in Sgr. B2, Orion A and W49. However, the system design is such that the receivers, control logic and power supplies can, and probably will, be divorced from the 22 GHz front end and telescope drive and used as a back end at the 26 metre antenna at Hartebeesthoek. The Hartebeesthoek dish with the Rhodes spectral line receivers could be used to study, for example, formaldehyde

(H_2 C O) at 4, 830 GHz.

This section is devoted to a description of the development, construction, testing and operation of the line receiver.

2. 1 After the front end mixer

The high frequency or front end section has been described in Chapter 1. When spectral lines are being observed (option A or B, Figure 1. 2) the IF signal from the 110 MHz amplifier in the Aerojet mixer is fed to a narrow band 30 MHz IF amplifier manufactured by RHG Electronics Laboratory and mounted on the front end base plate. The RHG amplifier has a manual gain control and facilities for AGC. The amplifier output has been tested using a spectrum analyser and results are shown in Table 2. 1

Table 2. 1

RHG NARROW BAND 30 MHz AMPLIFIER

Centre frequency	28, 5 MHz
3 dB points	22, 5 ; 34, 6 MHz
3 dB bandwidth	12, 1 MHz
Gain at 31 MHz	79 dB maximum
	64 dB minimum

These figures are in agreement with the manufacturer's specifications (see Appendix B1).

The amplified IF signal is fed via RG - 8/U 50 ohm cable to the telescope receiver and into a main distribution amplifier as shown in Figure 2. 1. This supplies up to ten receiver trays each containing a second distribution amplifier feeding ten channels per tray. Each channel is effectively a

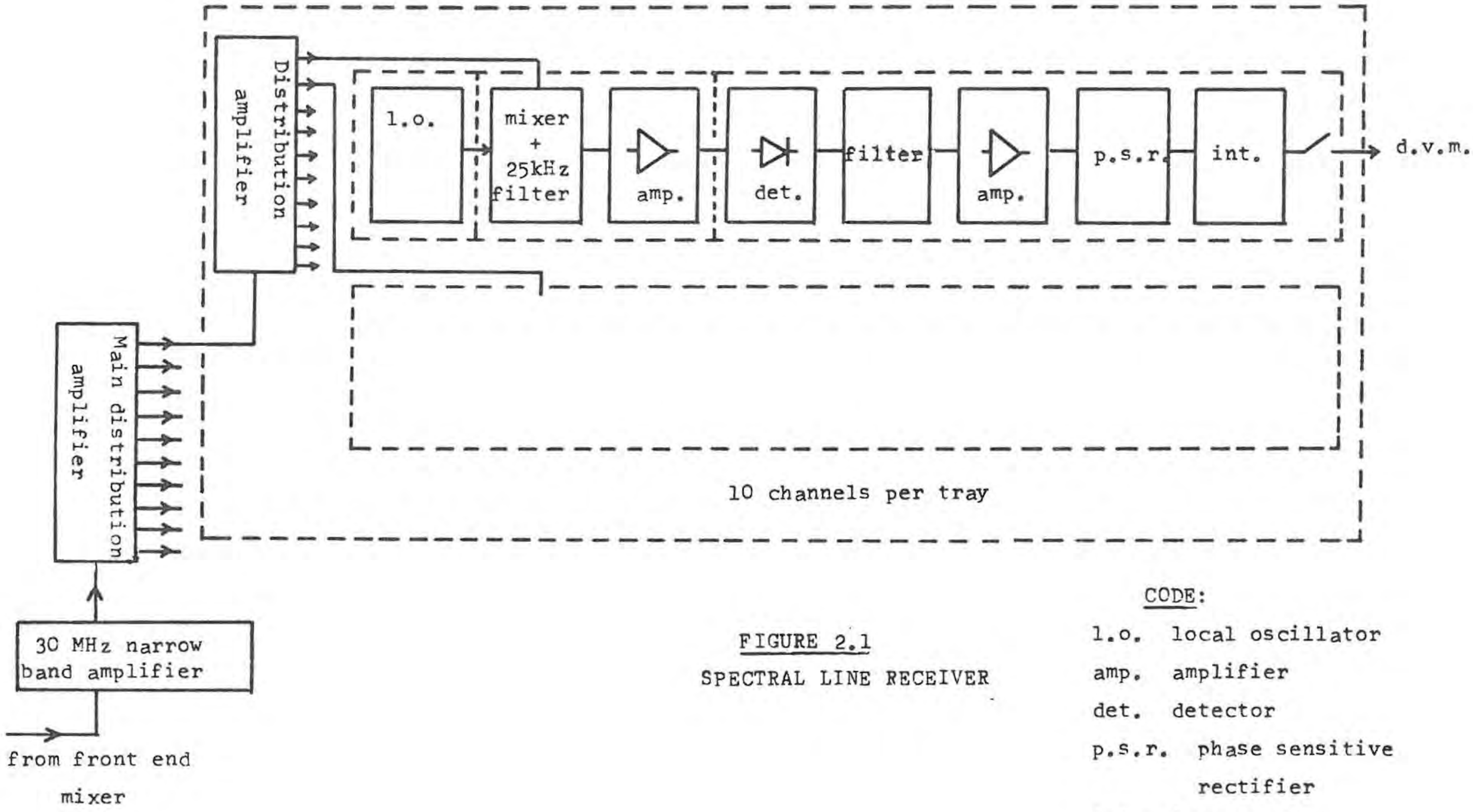

FIGURE 2.1

SPECTRAL LINE RECEIVER

CODE:

l.o. local oscillator

amp. amplifier

det. detector

p.s.r. phase sensitive rectifier

int. integrator

d.v.m. digital voltmeter

fixed frequency receiver.

2.2 The line receiver local oscillator

The general components of a line receiver channel are shown in Figure 2.1. The local oscillator is similar to a Colpitts oscillator but incorporates a crystal as part of the resonant circuit as shown in Figure 2.2. Crystal controlled oscillators have very good frequency stability.

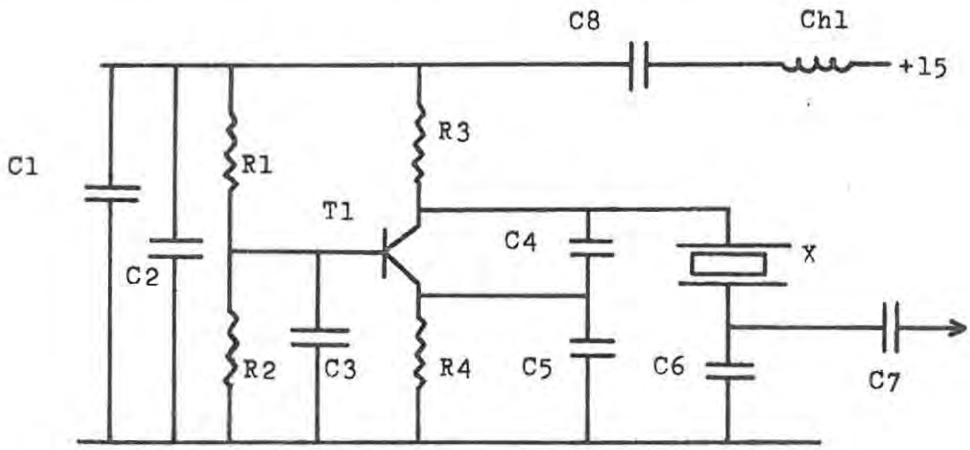

R1	4K7	C1	1 nF	C6	22 pF	Ch1	750mH
R2	1K2	C2	1 μF	C7	33 pF	T1	BC 109
R3	680	C3	0,01 μF	C8	1 nF		
R4	220	C4,C5	100 pF				

FIGURE 2.2
LOCAL OSCILLATOR

Components R1, R2 and C6 determine a suitable output free of harmonic distortion. Baart (1973) has determined the chosen values for a clean sine output of 3,5 volts peak to peak. The crystals were manufactured by STC and range in the fifty channels from 28,8 MHz to 31,25 MHz with a separation of 50 kHz. The printed circuit (PC) board has been designed so that the crystal may be changed without removing the local oscillator. The oscillator is shielded from the remainder of the channel (see Appendix B2).

2.3 The mixer, 25 kHz low pass filter and amplifier

The mixer makes use of an RCA 40673 Silicon metal oxide field effect transistor (MOSFET). By using a MOSFET the design minimizes spurious responses that occur when harmonics of the local oscillator signal are mixed with harmonics of unwanted incoming signals to produce difference frequencies within the passband.

The mixer, filter and amplifier circuit is shown in Figure 2.3. The local oscillator signal goes to gate 2 and the input signal to gate 1 of T2. R7 is set at 50 ohms to match the RG - 174/U cable from the distribution amplifier and R6 is 1 kilo-ohm, that is, 20 times R7 for attenuation in the reverse direction.

A Bode plot for the 25 kHz low pass filter appears as Figure 2.4. The 3 dB and 6 dB points occur at 23 kHz and 27 kHz respectively.

The gain of the operational amplifier may be adjusted by the potentiometer P1. The output of this stage is normally set at 2 volts peak to peak for proper detector action. This amounts to a gain of about 100.

2.4 The detector, bandpass filter and amplifier driver

The receiver circuit immediately following the mixer amplifier is shown in Figure 2.5. The design is based on a circuit developed at Cambridge University. The detector is an OA95 silicon diode. R16 is a return to earth after the diode and is chosen slightly larger than R15. Components R17 to R20, C17 to C19 make up a bandpass filter. The filter is designed for a particular switching frequency. The more bandwidth included, the more noise is also included and the signal to noise ratio is degraded. However if only the first harmonic of the switch frequency is included the efficiency of the receiver is reduced.

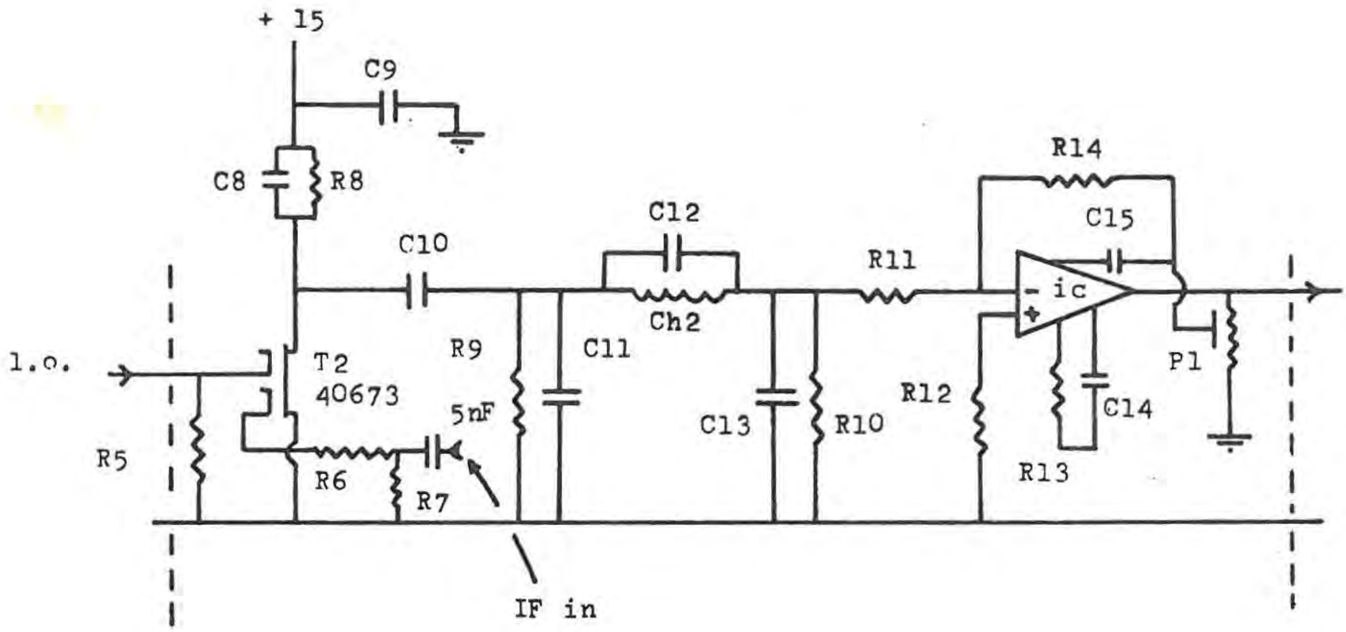

R5	100k	C8	0,022 μF	T2	40673
R6,R8	1K	C9	1nF	Ch2	2,5mH
R7	50	C10	2,2 μF	ic	709
R9	680	C11,C13	0,03 μF	P1	10k
R10,R11,R14	820	C12	0,004 μF		
R12	470	C14	470pF		
R13	1k	C15	47pF		

FIGURE 2.3

MIXER,25kHz FILTER,AMPLIFIER

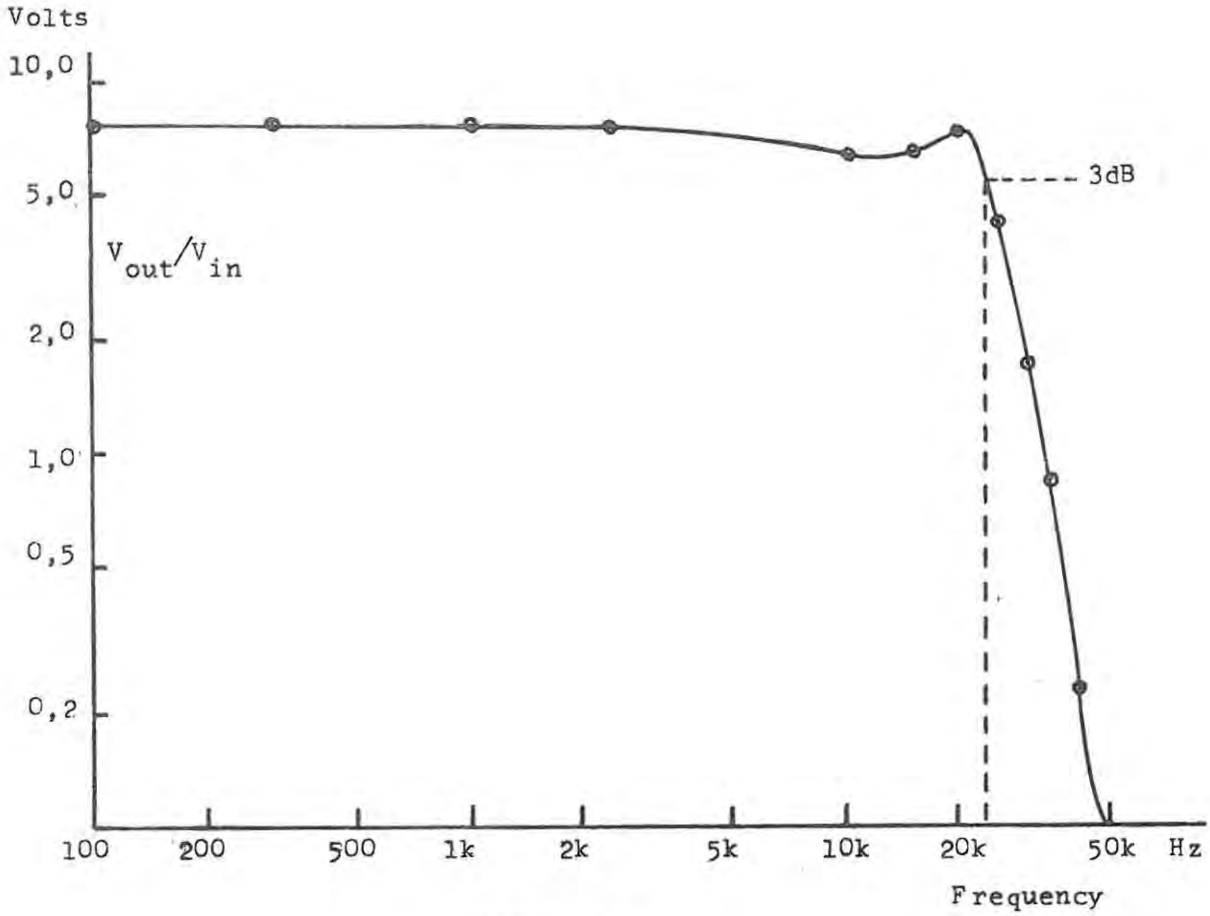

FIGURE 2.4
BODE PLOT
25kHz LOW PASS FILTER

The filter has been optimized to include the first and third harmonics of the switching frequency. The fifth harmonic should be 6 dB down. The third harmonic is included to approximate a square wave. The filter was initially designed for a switching frequency of 19 Hz. After tests on frequency switching and in particular on the front end Gunn oscillator lock acquisition time (see Chapter 1) the filter was redesigned for a switching frequency of 95 Hz. The switching frequencies have been chosen away from any harmonic of the mains frequency. Bode plots of both designs appear as Figure 2.6. For the 19 Hz filter the 3 dB and 6 dB points occur at 56 Hz and 98 Hz. The equivalent points for the 95 Hz filter are at 290 Hz and 520 Hz.

The amplifier has a gain between unity and almost infinity and the printed circuit board has been designed so that the gain control potentiometer P2

FIGURE 2.5

DETECTOR, BANDPASS FILTER, AMPLIFIER

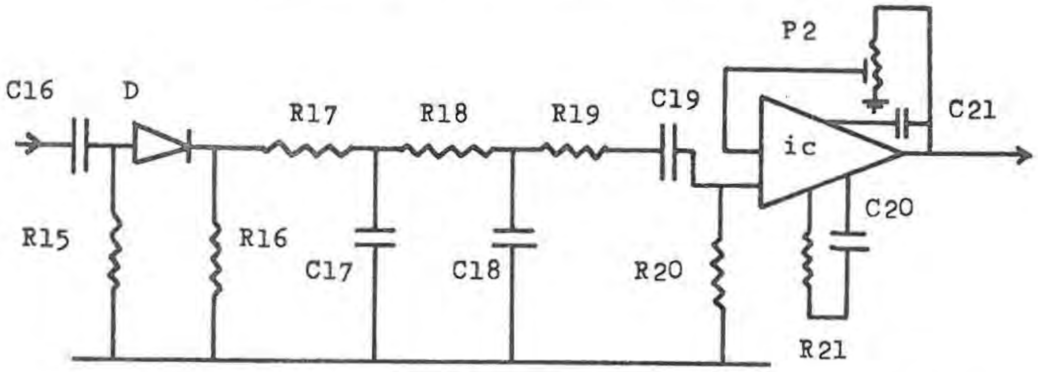

R15	3k3 Ω	C16	0,47 μF	D	OA95
R16	3k9	C17	0,039 (95Hz)	ic	709
R17	8k2		0,22 (19Hz)	P2	10k
R18	20k (95Hz)	C18	0,015 (95Hz)		
	18k (19Hz)		0,1 (19Hz)		
R19	10k	C19	0,47		
R20	100k	C20	0,002		
R21	1k5	C21			

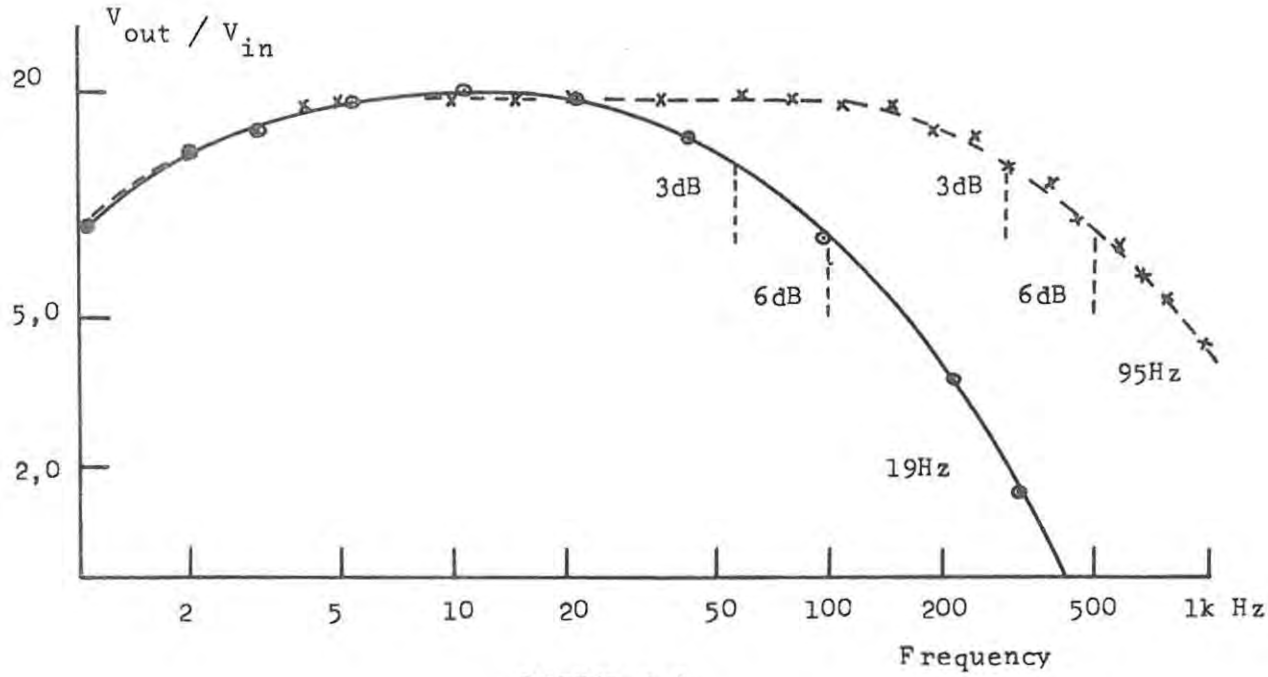

FIGURE 2.6

BODE PLOTS

BANDPASS FILTERS FOR 19Hz AND

95Hz SWITCHING FREQUENCIES

is accessible from the receiver tray front panel.

2.5 Phase sensitive rectification and the integrator

Figure 2.7 illustrates the remainder of the receiver circuit comprising the phase sensitive rectifier (P.S.R.), integrator and the reset and output control.

The receiver input is frequency switched (see Chapter 1) on and off the spectral line source by switching the tuning voltage applied to the varactor in the Gunn oscillator in the front end. This procedure reduces the effect of gain variations if the switch frequency is such that the gain change in one cycle is small. The source signal power is square wave amplitude modulated because the information from the source only enters the spectral line channels during alternate half-cycles. This modulated signal is detected, filtered and amplified by the circuit depicted in Figure 2.5 and then passes to the phase sensitive rectifier or synchronous demodulator.

The field effect transistor, T3, is switched synchronously with the Gunn oscillator. In an "on" state, when the receiver input is frequency switched onto the source, the f.e.t. has a drain to source resistance of about 50 ohms and the integrator input is effectively at earth. The capacitor C22 charges up according to the random noise and source signal strength. In an "off" state, the receiver is frequency switched off the source and the f.e.t. has a very high resistance to earth. The voltage at the integrator input is that at the output of the post-detector amplifier minus the voltage on the capacitor. Random noise has the same effect on average for alternate half-cycles so only the component at the switch frequency will not be integrated to nearly zero. The integrator output will be positive or negative depending on the phase of the P.S.R. switch signal with respect to the front end switch signal and depending on whether a voltage change applied to the Gunn varactor switches the receiver on or off the source.

A μA 740 operational amplifier is used as an integrator. Potentiometer P3 provides a coarse drift control accessible from inside the receiver

FIGURE 2.7

PHASE SENSITIVE RECTIFIER,
INTEGRATOR, RESET,
OUTPUT CONTROL

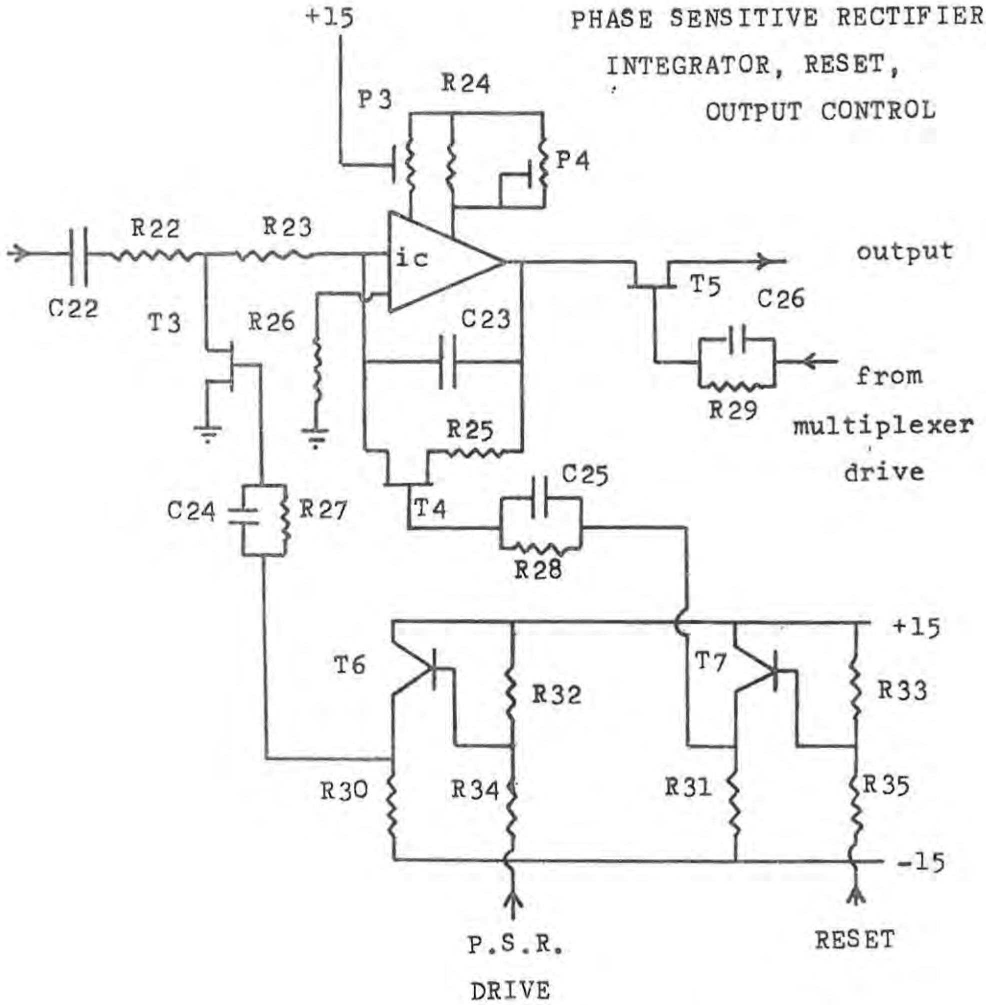

R22 220kΩ (19Hz)
R23 44k (95Hz)
R24 1k
R25 1k (½watt)
R26 330k (19Hz)
68k (95Hz)
R27, R28, R29 10M
R30, R31 56k
R32, R33 22k
R34, R35 100k

C22 0,47 μF
C23 4,7 μF
C24, C25, C26 22 pF
P3, P4 10k
T3, T4, T5 2N4093
T6, T7 3638A
ic 740

tray. The printed circuit board was designed so that the fine drift control (P4) may be adjusted through the receiver tray front panel.

Field effect transistors are used to provide integrator reset and output control. The P.S.R., reset and channel select signals are provided by the receiver control unit via a tray control and multiplexer circuit (Way-Jones, Mountfort, 1975). Transistors T6 and T7 control the P.S.R. and reset voltage levels applied to the f.e.t. gates.

2.6 Receiver box design and construction, receiver tray layout and power supplies

It is very important to prevent interaction between the channels and therefore they have been mounted individually in shielded boxes. The size and structure of the receiver boxes are shown in Appendix B2. The box is made of five separate pieces of aluminium and has a detachable lid. The sections are welded to make up three shielded compartments which contain the oscillator, mixer and integrator printed circuit boards. The IF input and P.S.R. signals are fed into the box via RG-174/U 50 ohm cable and SMC connectors. The power supplies, reset and output lines enter via miniature feed through connectors.

The tray layout is shown in Appendix B3. Each receiver tray contains ten channels with ten contiguous local oscillator crystals 50 kHz apart, +15 V, +12 V, -15 V regulators, an IF distribution amplifier, a receiver control and multiplexer circuit and a P.S.R. distribution unit.

The receiver tray base is heated by four 750 W toaster elements in series. The elements are enclosed in two 5 mm thick asbestos sheets. The temperature in the tray is regulated by a thermistor connected to a heater control circuit mounted in power supply tray 2 (see Section C and Appendix B4).

The temperature is adjustable and is normally maintained at 42°C.

2.7 Spectral line receiver testing and operation

Twenty spectral line channels have been built and installed in receiver trays to date. Of the remaining thirty receivers, all the local oscillator boards and fifteen integrator boards have been constructed. The installation of all fifty channels should be completed shortly.

The twenty channels installed have been thoroughly tested over a period of several months. Reliability has been excellent in that no component failure has occurred.

The final section of part A of this chapter thus presents test results and indicates the success of the basic receiver design.

An estimate of integrator drift was of immediate interest after the completion of the first receiver. Baart (1973) has estimated that drifts of the order of 10 millivolts per 100 seconds integration would be desirable. This figure is comparable with the smallest source signal output expected. This drift rate was reached and maintained over a period of some twenty integrations under non-stable temperature conditions.

Figure 2.8 presents a pen recorder trace of integrator output over a period of six hours after installation in the temperature controlled receiver trays. The integrator is zeroed after each 100 second integration. A rate of 10 millivolts per 100 seconds was maintained over some 130 of 210 one hundred second integrations. Approximately 45 integrations had drifts less than 20 millivolts and 34 integrations had drifts less than 40 millivolts. These rates are acceptable as steady integrator drift may be subtracted out by changing the phase of the P.S.R. switch signal on

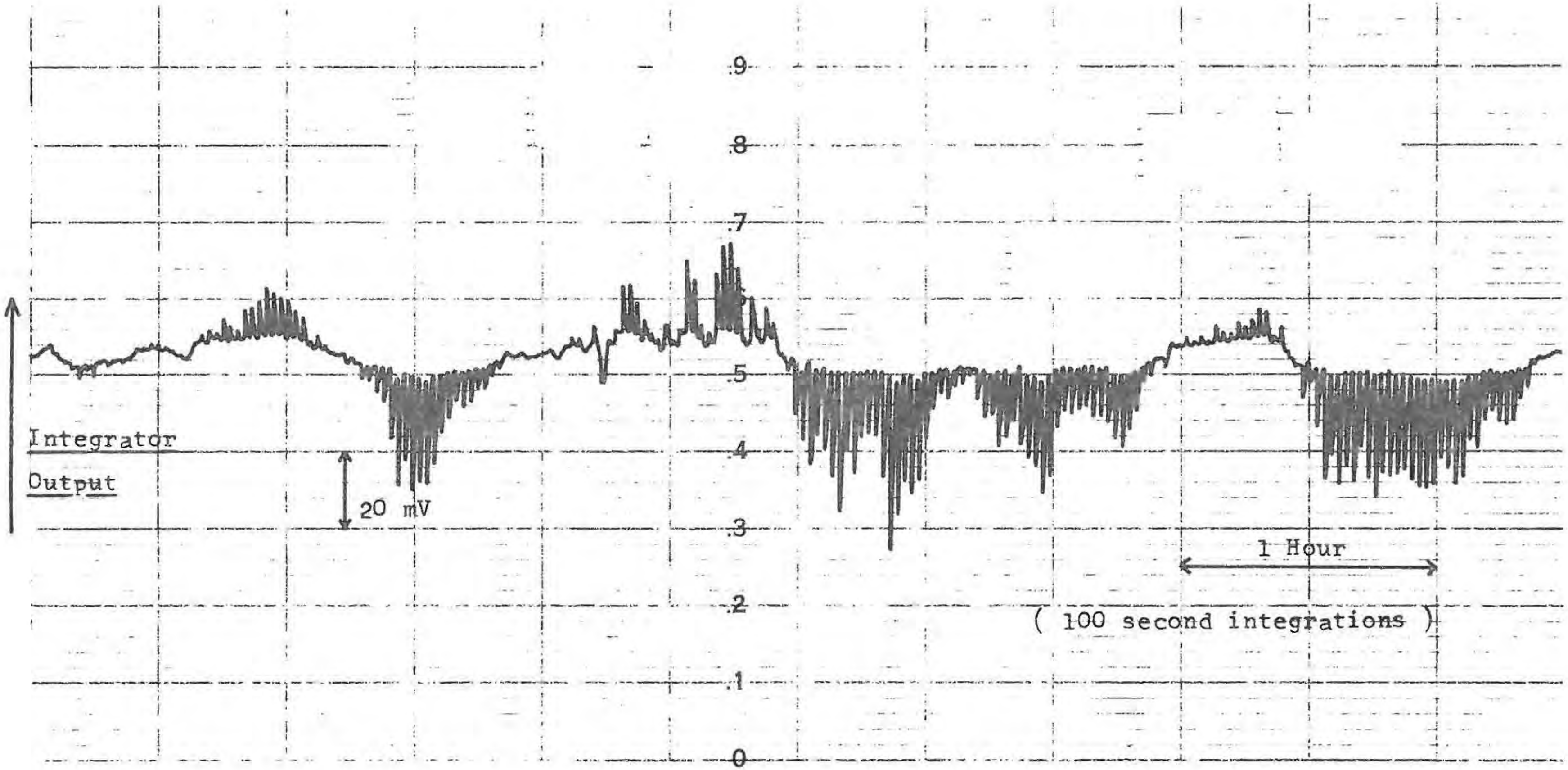

FIGURE 2.8

RECEIVER INTEGRATOR DRIFT

alternate runs.

The operational amplifier chosen as an integrator (μA 740) is not the most satisfactory in terms of drift figures but was used because it is inexpensive.

Channel interaction was tested by mounting two channels with minimum frequency separation (50 kHz) next to each other. Dual pen recorder traces of integrator output indicated no detectable mutual interaction. As an additional precaution the channels are normally mounted so that channels close in frequency are physically widely separated.

Prior to the installation of the front end behind the telescope dish the entire receiver system (see Figure 1. 2 and Figure 2. 1) was bench tested. The reserve Varian Gunn oscillator was mounted in place of the main horn. This heavily attenuated oscillator acted as a test source. The local oscillator was tuned and locked to a frequency 30 MHz away from that of the test source. The ten spectral line receivers under test performed as expected. Instruments monitoring the output of the post detector amplifiers and integrators could clearly detect the frequency drift of the test source from one receiver channel to the next.

The receiver control unit has a facility for displaying all the receiver channel outputs simultaneously on an oscilloscope in the form of a, so called, histogram. This feature has been used to perform receiver gain and drift adjustments and provides a means of photographically recording receiver integrator outputs.

Figures 2. 9 (a to d) illustrate the detection in separate channels of an externally pulse modulated 30 MHz test signal injected into the twenty receivers through the distribution amplifiers. The modulation takes the form of a 95 Hz square wave effectively simulating front end switching.

The photographs indicate the lack of channel interaction, except where the test signal is tuned to overlap two adjacent channels. In Figures 2.9 (a, b and c) the 30 MHz signal has been tuned to appear, in turn, in channels 1, 4 and 6 respectively. There was a slight signal overlap in Figure 2.9(d) and channels 12 and 13 responded.

Finally the twenty receivers were tested with the front end installed and a test transmitter sending a signal at the telescope dish. Unfortunately since installation both electromechanical Varian Gunn oscillators have developed faults. The L-Gunn Varactor diode appears to be damaged and voltage tuning and hence phase locking is not possible. This oscillator has been returned to Varian. Later tests performed on the total power receiver (see Section B) indicated the presence of substantial standing waves in the front end. These have been attributed to the replacement oscillator (S-Gunn) apparently generating side bands. This Gunn has in turn been replaced by the Mid-Century Microwavegear oscillator. The S-Gunn is presently being used as a test transmitter.

Final spectral line receiver tests were thus performed without a phase locked local oscillator and with an unstable test oscillator. Figures 2.10 (a to d) illustrate the detection of the rapidly drifting transmitter.

Individual channels respond to the drifting signal until finally, as shown in Figure 2.10 (d), the integrators saturate.

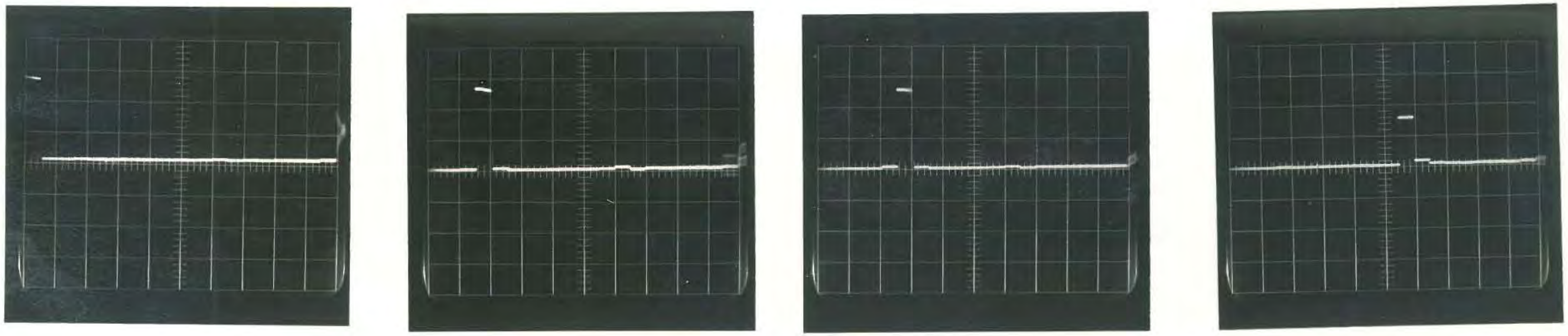

a b c d

FIGURE 2.9(a to d)

30 MHz signal injected into 20 channels, tuned to appear in channels 1,4,6,12.

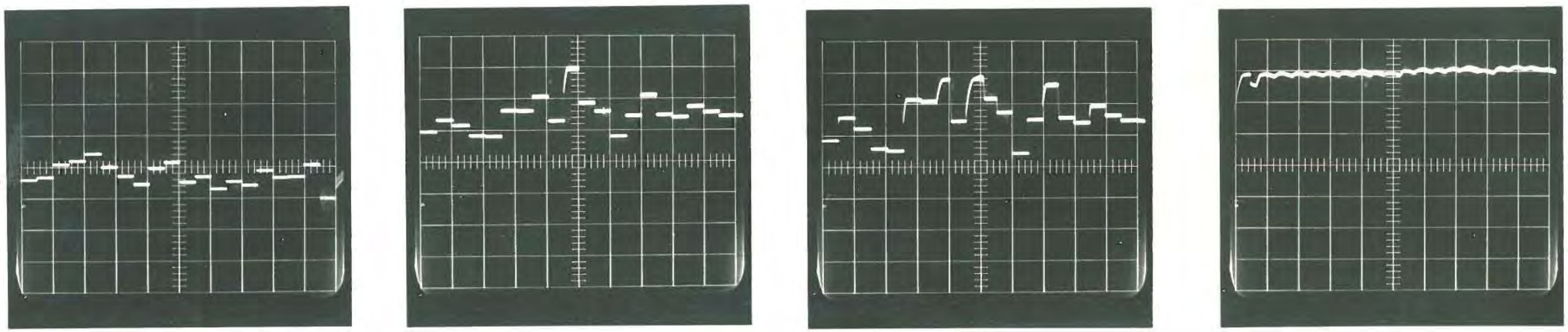

a b c d

FIGURE 2.10(a to d)

Detection of rapidly drifting test transmitter.

B The continuum receiver

The development of the spectral line receiver in order to observe 22 GHz water vapour sources was discussed in Section A. An alternative use of the telescope is the study of 22 GHz continuum sources. A total power receiver is required for this purpose and has been constructed. The receiver is essentially similar to one channel in the line receiver. The bandwidth of the continuum receiver should be as broad as possible but in practice it is determined by the bandwidth of the amplifier built into the Aerojet mixer, that is, 100 MHz.

The increase in bandwidth over that of the line receiver and the fact that both signal and image channels of the Aerojet mixer can be used for continuum studies result in nearly a one hundred-fold increase in sensitivity (see Section 1. 6).

First results from the radio telescope were gained using this receiver. The continuum receiver has been used for the alignment and focussing of the antenna and in Chapter 6 estimates of the half power beam width and aperture efficiency will be presented.

2. 8 After the mixer

During total power receiver operation the IF signal from the 110 MHz amplifier in the mixer is fed to a wide band amplifier manufactured by Trontech Inc. and mounted on the front end base plate. The amplifier has a gain of 62 dB over the bandwidth of the mixer. (This amplifier is being replaced by one manufactured by Avantech with a bandwidth of 500 MHz and a gain of 70 dB. The replacement amplifier also has facilities for up to 15 dB of AGC).

The amplified signal is then carried by 50 ohm cable directly to the continuum receiver illustrated in Figure 2.11. The continuum sources of interest have a wide range of signal strengths. Emissions from the Sun and Moon, for example, can saturate the receiver very rapidly whilst signals from Mars or Mercury can only be recorded after several hours of observation. After detection the signal is therefore fed to two separate circuits, the operation of which depends on signal strength. The, so called, strong source monitor is generally used for calibration purposes and for the detection of 22 GHz emission from the Sun. The circuit consists of a variable time constant smoothing network followed by a calibrated output meter. Certain measurements, for example of beam patterns, can be performed more accurately by using a smoothed output rather than a recorder which is zeroed after pre-set intervals. The second circuit is very similar to the line receiver integrator section. Phase sensitive rectification is again used but beam switching rather than frequency switching takes place at the front end (see Figure 1.2). The mixer input is switched between the main horn pointed on source and the secondary horn pointed off source. The integrator has been modified to allow the option of fixed integration times as in the line receiver or smoothing circuits with 1, 3, 10 or 20 second time constants.

Both the integrator and strong source outputs are fed to a pen recorder driver. Alternatively outputs may be recorded on paper tape or read directly into an on-line computer.

2.9 Receiver tray layout

The continuum receiver tray is placed above the spectral line trays and consequently has two heater units, one in the base and one in the lid. The spectral line receiver trays do not require heated lids because the heated base of the tray above effectively counteracts any heat loss.

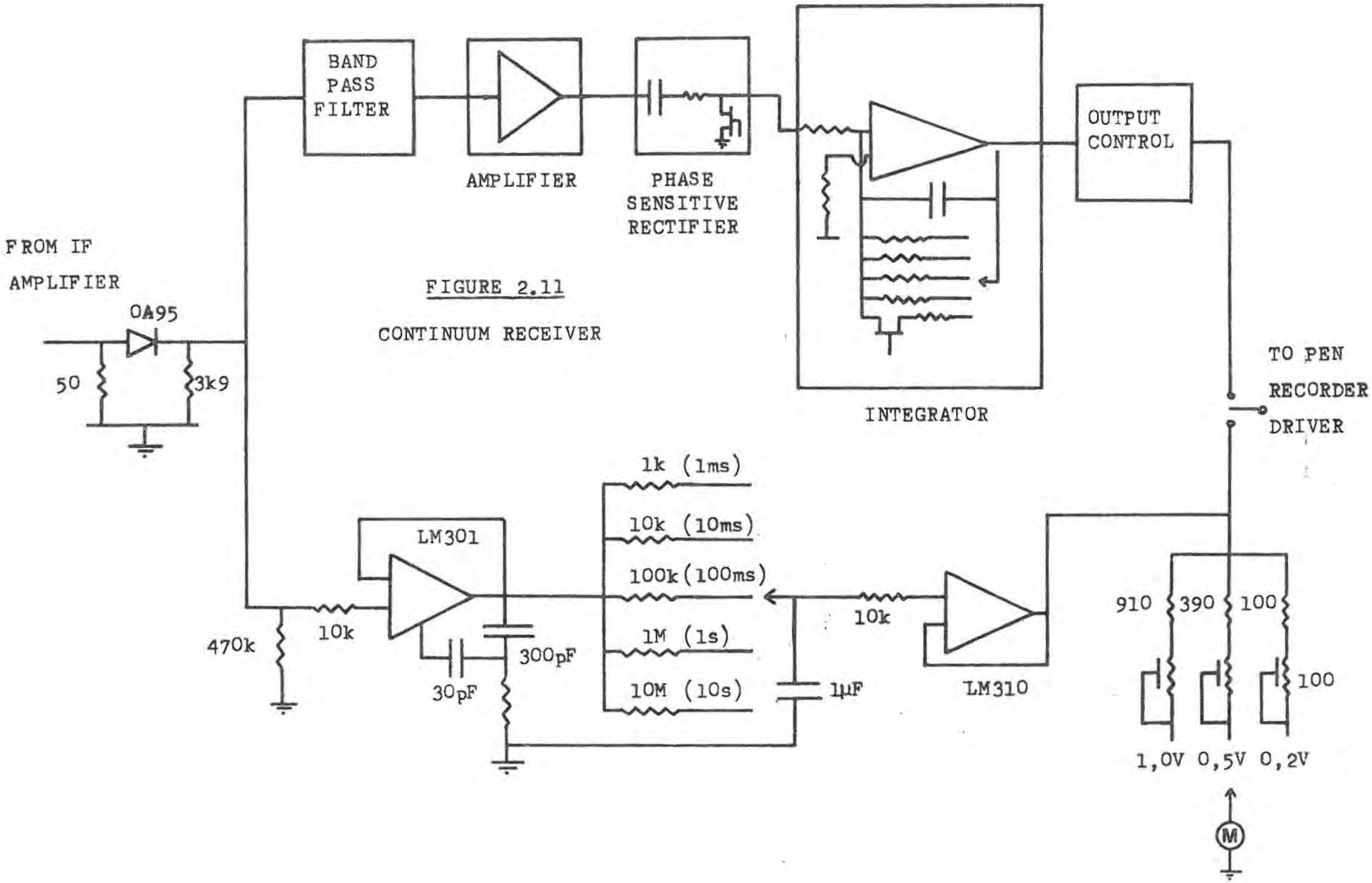

FIGURE 2.11

CONTINUUM RECEIVER

The strong source and pen recorder driver circuits have been built onto Vero boards and are mounted vertically in the tray. The integrator circuit has been built in a section of a spectral line receiver box. The integrator coarse and fine drift controls, amplifier gain control, smoothing circuit selector switches and pen recorder controls are mounted on the front panel.

2.10 Testing and calibration

The receiver was bench tested prior to the installation of the total power option of the front end behind the telescope dish. Initial measurements were carried out by firing the 22 GHz noise source. The integrator output, for a particular gain setting of the post detector amplifier, may be calibrated against the amount of attenuation in the noise source line. During measurements made on the receiver using a spectrum analyser with the front end in location the L-Gunn local oscillator developed a serious fault. The varactor diode appeared to be damaged and the replacement Varian Gunn was installed.

On the 5th September 1974 22 GHz emission from the Sun and Moon was detected. An estimate of the aperture efficiency of the telescope was made by comparing detector outputs resulting from signals from the Sun and the calibrated noise source.

A test transmitter was constructed using the Mid-Century Microwavegear Gunn. The transmitter was placed 100 metres from the telescope and 10 metres above ground level. This arrangement was used to determine the antenna half power beam width. The results of the measurements are presented in Chapter 6.

C The receiver and logic power supplies

2.11 Power supply layout and control

The receiver and logic power supplies are enclosed in three trays in the base of the receiver and telescope control rack. The general arrangement and interconnection of the trays is shown in Appendix B4.

Very stable but fairly low current supplies are required by the spectral line and continuum receivers. A 400 W constant voltage transformer (CVT) in tray 1 feeds receiver supply circuits in tray 3 which provide +20, -20, +15, -15 and +5 volts at the receiver trays. Each receiver tray contains +15, -15 and +12 volt regulators.

In contrast the logic circuits demand very large currents. Tray 2 contains the logic power supply circuits and these are fed by an 850 W CVT in tray 1. The voltages provided are +24, +15, - 15 and +12.

Tray 2 also contains ten heater temperature control boards for the receiver trays and a battery charger circuit. A battery is used to maintain the U. T. and sidereal time clocks during power failures.

The power supply and heater control switches are on the front panel of tray 3.

Detailed circuit diagrams and component lists are available for maintenance purposes.

CHAPTER THREE

TRACKING A RADIO SOURCE

3.1 Precession correction : Epoch to year of observation

3.2 Day number correction : Beginning of year to day of observation

3.3 Calculation of local apparent sidereal time

3.4 Coordinate transformation

3.5 Time of transit

CHAPTER THREE

TRACKING A RADIO SOURCE

The Rhodes radio telescope mount is calibrated on the basis of a horizon coordinate system. A plane through the observing point parallel to the horizon is the plane of reference. The coordinates of a source are given by the azimuth, the horizontal angle measured clockwise from north, and the altitude, the elevation angle measured upward from the horizon.

Radio source positions are given in terms of equatorial coordinates, usually for epoch 1950, 0. In this system the earth's equator is the plane of reference and the source coordinates given are the declination, δ, the angle between the celestial equator and the source and the right ascension, α, the angle between the vernal equinox and the great circle through the celestial poles and source (the source hour circle). The vernal equinox is towards the constellation Pisces. Some years ago it was in the direction of Aries because of the precession of the Earth's axis. For this reason the vernal equinox is often termed the first point of Aries.

Accurate values are thus required of the altitude and azimuth of a given source at any given time for calibration and tracking purposes.

In the first instance, a precession correction from epoch 1950, 0 to, say, 0^h U.T. January 1st 1975 is necessary. If accurate values for α, δ 1975 are available then in some instances day number corrections giving reduction for precession, nutation and aberration may be valuable. The day number corrections are usually not more than a few seconds of arc and hence are not necessary with our present telescope which has a half power beam width of 27 minutes of arc.

The apparent (corrected) α and δ must be transformed to an alt-azimuthal coordinate system and it is useful if these coordinates may be adjusted for an incremented time throughout a period of observation. The time of transit of a source may also be required.

This chapter presents in logical order the procedures to be followed. The mathematical principles and detailed examples are given. Appendix C lists operations for a computer programme that was written for the Hewlett-Packard Model 10 calculator. The programme calculates precise values of the altitude and azimuth of a source at any time of observation.

3.1 Precession correction : Epoch to year of observation

The ~~notion~~ notation followed is that adopted by Kraus (1966), page 37. Similar equations may be found in the Astronomical Ephemeris for the year 1975, page 9.

The coordinates α_1, δ_1 (epoch 1) are to be precessed to new coordinates α_2, δ_2 N years later at epoch 2. $\Delta\alpha$ and $\Delta\delta$ are calculated from

$$\Delta\alpha = (m_1 + n_1 \sin \alpha_1 \tan \delta_1)\, N \quad \text{seconds (time)} \qquad 3.1$$

$$\Delta\delta = (n_1 \cos \alpha_1)\, N \quad \text{seconds (arc)} \qquad 3.2$$

where m_1 and n_1 are the annual precession in α and δ respectively for epoch 1. Changes $\Delta\alpha'$ and $\Delta\delta'$ are calculated from

$$\Delta\alpha' = [m_2 + n_2 \sin(\alpha_1 + \Delta\alpha) \tan (\delta_1 + \Delta\delta)]\, N \quad \text{seconds (time)} \qquad 3.3$$

$$\Delta\delta' = [n_2 \cos(\alpha_1 + \Delta\alpha)]\, N \quad \text{seconds (arc)} \qquad 3.4$$

where m_2, n_2 are precession constants for epoch 2.

The corrected α_2, δ_2 are given by

$$\alpha_2 = \alpha_1 + (\Delta\alpha + \Delta\alpha')/2 \qquad 3.5$$

$$\delta_2 = \delta_1 + (\Delta\delta + \Delta\delta')/2 \qquad 3.6$$

Consider as an example the star Sirius (α CMa) 1950, 0 precessed to 1973, 0.

$$\alpha_1 = 6h\ 42m\ \ 56,73s = 100,7364 \text{ deg.}$$

$$\delta_1 = -16 \text{ deg } 38m\ \ 46,4s = -16,6462 \text{ deg.}$$

m_1 (1950) = 3, 07327 seconds (time)

n_1 (1950) = 1, 33617 seconds (time) = 20, 0426 seconds (arc)

N = 23

Hence, $\Delta\alpha$ = 61, 6576 seconds (time) = 0, 017127 hours

$\Delta\delta$ = - 85, 8759 seconds (arc) = -0, 02385 deg.

m_2 (1973) = 3, 07370 seconds (time)

n_2 (1973) = 1, 33604 seconds (time) = 20, 0406 seconds (arc)

Hence $\Delta\alpha'$ = 61, 6623 seconds (time) = 0, 017128 hours

$\Delta\delta'$ = -87, 8955 seconds (arc) = -0, 02442 deg.

thus

$$\alpha_2 = 6h\ 43m\ 58s$$

$$\delta_2 = -16 \text{ deg. } 40m\ 13s$$

This result may be compared with figures for α CMa from the Astronomical Ephemeris 1973

$$\alpha = 6h\ 43m\ 57,5s \qquad 3.7$$

$$\delta = -16 \text{ deg. } 40m\ 41s$$

The errors involved are thus of the order of 30 seconds of arc.

3.2 Day number correction : Beginning of year to day of observation

The corrections excluding proper motion and second order terms are (Astronomical Ephemeris 1975, page 544)

$$\alpha = \alpha_o + Aa + Bb + Cc + Dd \qquad 3.8$$

$$\delta = \delta_o + Aa' + Bb' + Cc' + Dd' \qquad 3.9$$

where

$a = m/n + \sin \alpha_o \tan \delta_o$ | $a' = \cos \alpha_o$

$b = \cos \alpha_o \tan \delta_o$ | $b' = -\sin \alpha_o$

$c = \cos \alpha_o \sec \delta_o$ | $c' = \tan \epsilon \cos \delta_o - \sin \alpha_o \sin \delta_o$

$d = \sin \alpha_o \sec \delta_o$ | $d' = \cos \alpha_o \sin \delta_o$

These are the Besselian star constants in seconds of arc. A, B, C, D are the Besselian day numbers and ϵ is the mean obliquity. m and n are the annual precession in α and δ .

Consider as an example Sirius at 0^h U. T. January 1st, 1973 given by 3. 7 corrected to March 5th, 1973.

α_o = 6h 43m 57, 5s = 100, 989583 deg.

δ_o = -16 deg. 40m 41s = -16, 678056 deg.

The Besselian day numbers for March 5th, 1973 may be found in the Astronomical Ephemeris for that year and are

A = 10, 434	B = -2, 861	C = -18, 112	D = 5, 561

Therefore

a = 2, 006497	b = 0, 057112	c = -0, 199002	d = 1, 024771
a' = -0, 190631	b' = -0, 981662	c' = 0, 697115	d' = 0, 054710

Thus

α = 6h 43m 57, 5s + 2, 00s = 6h 43m 59, 5s

δ = -16 deg. 40m 41s - 11, 5s = -16 deg. 40m 52s

This result may again be compared with accurate data from the Star Almanac for Land Surveyors which gives monthly reductions.

α = 6h 43m 59, 2s

δ = -16 deg. 40m 54s

The errors involved are approximately 0, 3 seconds (time) in right ascension and 4 seconds of arc in declination.

3. 3 Calculation of local apparent sidereal time

The local apparent sidereal time is calculated by adding to the Greenwich apparent sidereal time the observation time (U. T.) in sidereal units and the observer's longitude.

Consider an observation of the Crab Nebula Pulsar made at 16h 14m 34s U. T. on January 14th, 1975 in Grahamstown.

Greenwich apparent sidereal time 0^h U. T.	7h	31m	21s
U. T. of observation	16	14	34
Correction of U. T. to sidereal units			
(x 0, 0027379093)		2	40
Longitude of site	1	46	5
	25h	34m	40s
local apparent sidereal time	1h	34m	40s

3. 4 Coordinate transformation

The transformation from an equatorial to a horizon system of coordinates, that is, from right ascension and declination to altitude and azimuth is performed by means of the following relations (Explanatory Supplement to the Ephemeris, 1961, page 26)

$$\text{local apparent sidereal time} - \alpha = h \qquad 3.10$$

$$\sin a = \sin \delta \sin \phi + \cos h \cos \phi \cos \delta \qquad 3.11$$

$$\sin \Theta \cos a = - \cos \delta \sin h \qquad 3.12$$

where

a is the altitude, Θ the azimuth and ϕ the observer's latitude.

Consider as an example the Crab Nebula Pulsar (α 5h 31m 30s; δ 21 deg. 59m [1950, 0]) at the time and place given in Section 3. 3. The application of equations 3. 1 to 3. 6, 3. 8 and 3. 9 gives the corrected α and δ as

$$\alpha = 5h\ 33m\ 3s \qquad 3.13$$

$$\delta = 21\ deg.\ 59m\ 58s$$

The local apparent sidereal time has been calculated in Section 3. 3 as

$$1h\ 34m\ 40s = 23,6667\ deg.$$

Hence $h = -59,5958$ deg.

Grahamstown's latitude, ϕ , is -33, 3 degrees and thus a and θ can be calculated from 3. 11 and 3. 12

$$a = 10\ deg.\ 45m\ 4s$$

$$\theta = 54\ deg.\ 29m\ 6s$$

The error in the corrected α , δ is approximately 30 seconds of arc and a simple check indicates that this produces an error in altitude and azimuth also of this order. The half power beam width of the telescope is 0, 45 $\pm$ 0, 02 degrees (see Section 6. 1) and the accuracy to which the telescope may be driven is one 2^{14} part of 360 degrees (Way-Jones, 1975), that is, 79 seconds of arc. Thus the estimation of source position is accurate to approximately 2 percent of the beam width and is twice as accurate as the minimum driving step.

3. 5 Time of transit

At transit the hour angle, h, is zero and hence from equation 3. 10 the right ascension is the local apparent sidereal time. The procedure is merely the reverse of that followed in Section 3. 3.

For example the transit time (U. T.) of the Crab Pulsar on January 14th, 1975 as observed from Grahamstown:

local apparent sidereal time (from equation 3. 13)	5h	33m	3s
longitude	- 1	46	5
	3	46	58
Greenwich apparent sidereal time 0^h U. T.	- 7	31	21
	20	15	37
Sidereal to U. T. (x 0, 0027304333)	-	3	19
U. T. of transit	20	12	18

CHAPTER FOUR

THE PARABOLIC DISH SURFACE

CHAPTER FOUR

THE PARABOLIC DISH SURFACE

4.1 The heat problem

The hyperbolic sub-reflector has been manufactured by shaping a 1/8th inch aluminium sheet onto a precisely cut wooden block. The procedure has been found to be accurate to within 0,1 mm but because of the thin sheeting the sub-reflector has one serious weakness. It is very sensitive to excessive heat.

During alignment of the sub-reflector supports the Cassegrain arrangement was inadvertently pointed at the Sun. Later measurements on the sub-reflector indicated that solar heat reflected from the aluminium surface of the main reflector had caused some distortion.

Clearly it was necessary to paint the surface of the main reflector to reduce the quantity of heat reflected and focussed onto the fragile sub-reflector. Measurements were required on the reflectivity of various white paint surfaces in the visible and infra-red regions.

4.2 Spectrometer measurements

Initially the equipment illustrated in Figure 4.1 was used to compare different surfaces. The surface under test was mounted in a vertical plane on the revolving table between the collimator and telescope of a spectrometer. A light source was directed through the collimator onto the surface and reflected light was detected by a Leybold photo diode mounted in place of the telescope eyepiece.

The apparatus was only intended to give order of magnitude extimates of reflectivity. A coherent light source, an He/Ne laser, and white light were used. The measurements obtained are shown in Table 4. 1

Table 4. 1

	He/Ne (mV)	White light (mV)
Incident light	39 ± 1	85
Equipment noise level	0, 003	0, 01
Polished aluminium surface	20 ± 2	67 ± 1
Rough aluminium surface	0, 008 ± 0, 001	0, 87 ± 0, 08
Matt-white painted surface	< 0, 003	0, 09

The measurements indicate that a painted surface reflects approximately 10% of the visible light given off by a rough aluminium surface but the detected energy is close to the noise limit of the equipment. Whilst not genuinely indicative of the reflectivity in the infra-red region the initial results gave an estimate of levels and indicated the detection problems. The properties of the surface in the infra-red region were of particular interest considering the heating effect and therefore a spectrophotometer operating from 2, 5 to 10 microns was used for further surface studies.

4. 3 The infra-red spectrophotometer measurements

Three paints were recommended by commercial agents.

a) Dulux Weatherguard brilliant white -external grained surface

b) Buffalo Bufftex -external coarse grained surface

c) Lac-R-spray - multipurpose matt white.

A Perkin-Elmer series 180 dual beam spectrophotometer was used to study the infra-red properties of these paints. The radiation path in this instrument is split by a half-silvered mirror. One beam passes through the sampling

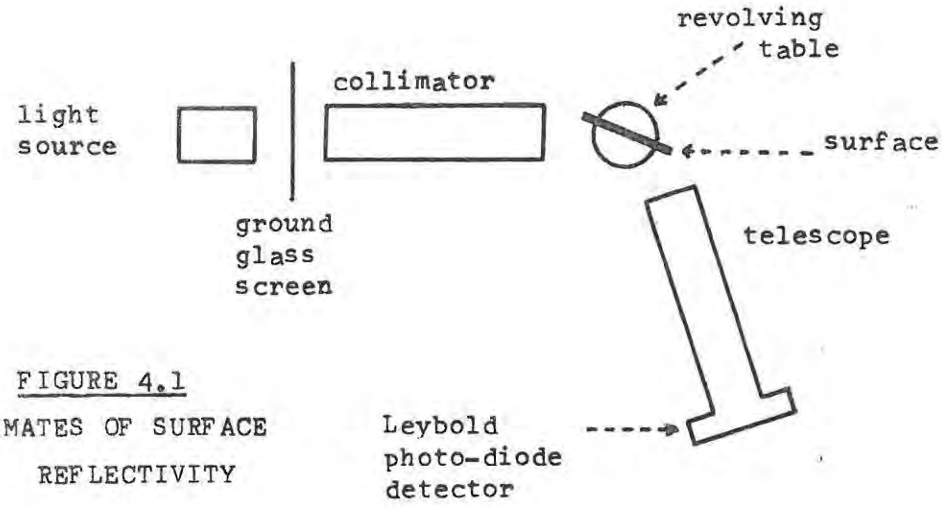

FIGURE 4.1

ESTIMATES OF SURFACE REFLECTIVITY

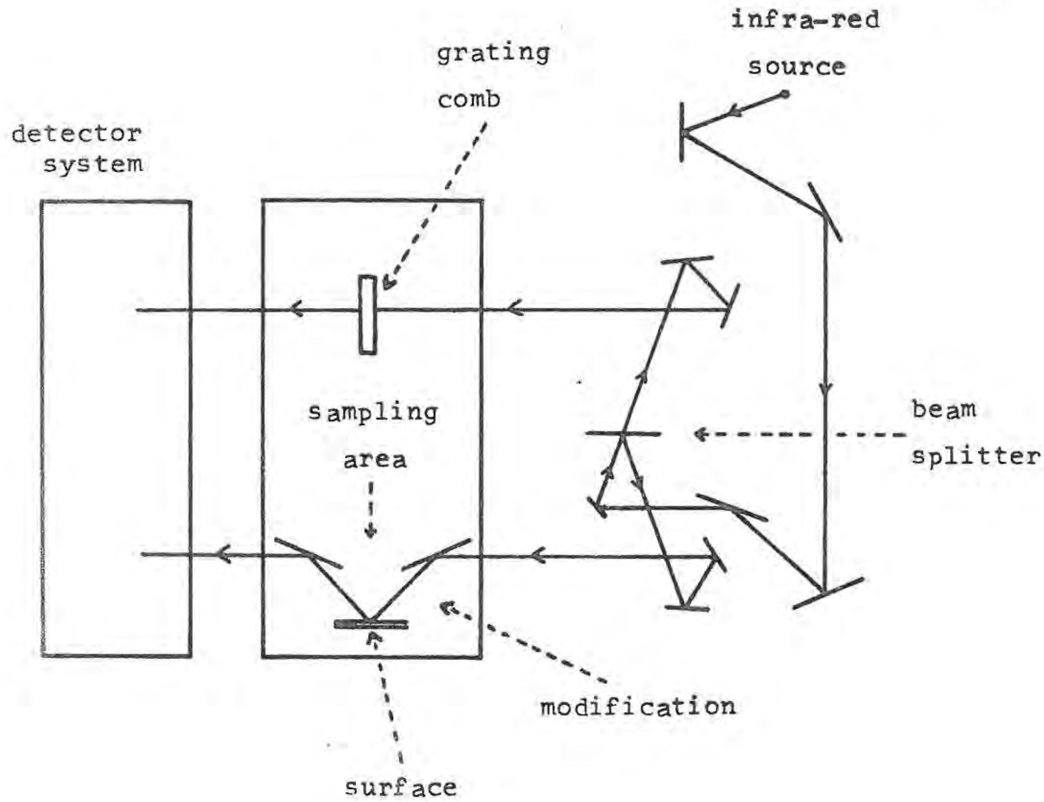

FIGURE 4.2

MODIFIED PERKIN - ELMER SPECTROPHOTOMETER area whilst a reference beam is directed through an adjustable grating comb. The arrangement is shown in Figure 4. 2. The instrument records the difference in the radiation intensity of the two beams. The purpose of the comb is to control the intensity of the reference beam and hence adjust the sensitivity of the instrument. Small changes in the absorption of radiation by a sample during a frequency scan can be recorded by adjusting the comb to equalize the sample and reference beams beforehand. Alternatively the comb can be adjusted to set a reference level and sample comparisons can be performed.

The instrument normally measures the degree of absorption of infra-red radiation in fine powdered samples. The energy transmitted through the sample is detected.

A sample and reflector support structure was thus designed and built to modify the path of the sample beam to enable the instrument to be used for reflectivity measurements. The sample and reflectors could be adjusted in three planes for maximum energy detection. The front silvered mirrors made for the modification were found to absorb some infra-red energy and they were later replaced by highly polished aluminium plates.

Initially a polished aluminium surface was studied to provide a reference. The grating comb in the second beam was adjusted for maximum sensitivity and a scan was performed from 2, 5 to 10 microns. The spectrophotometer scan is shown in Figure 4. 3 (upper trace).

The polished surface was removed from the sampling area and replaced with a rough aluminium surface. The comb was readjusted and a reference level was recorded. Finally the three painted samples were compared with the rough surface. A scan was performed on the Weatherguard sample

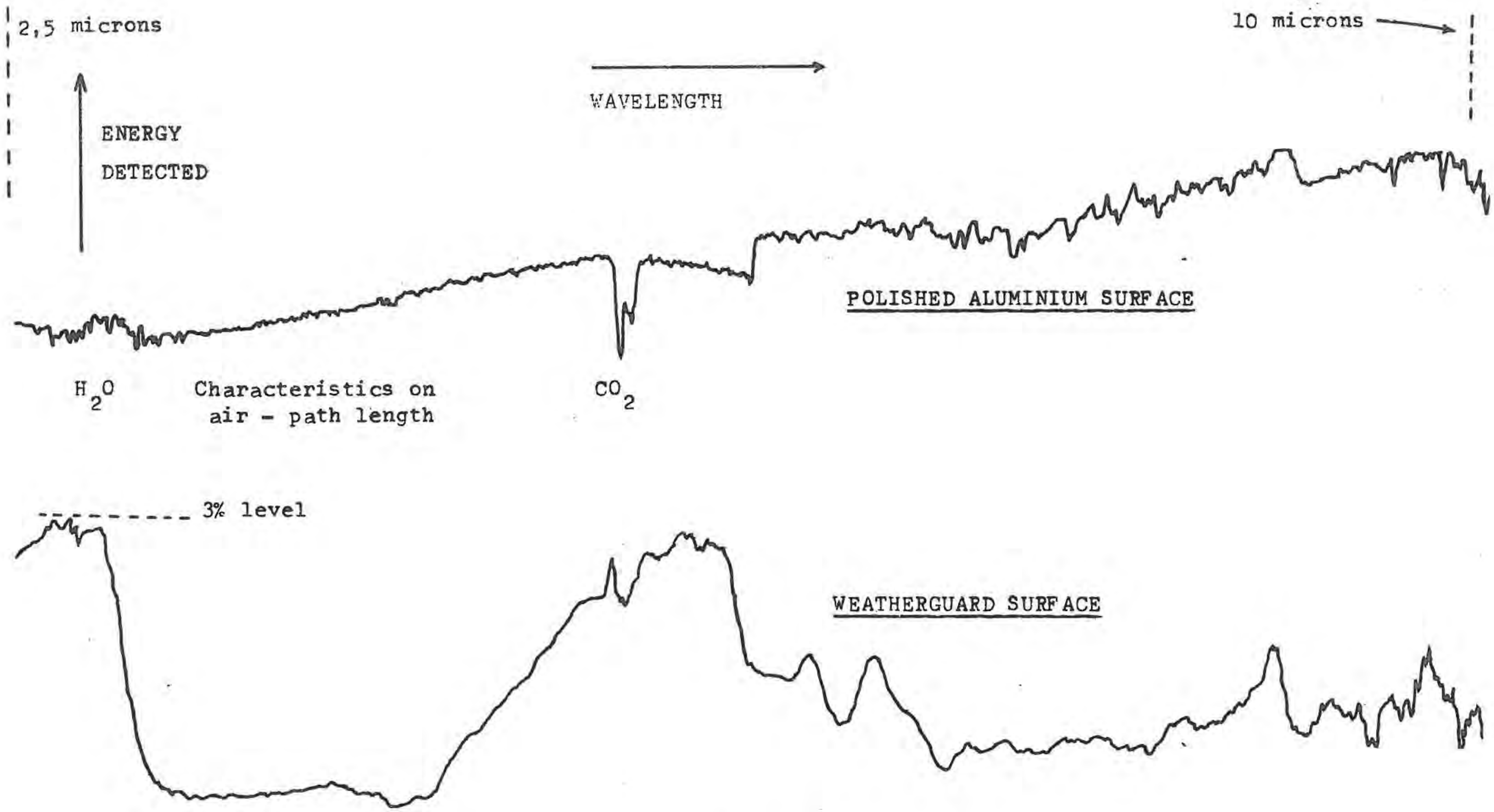

FIGURE 4.3

SPECTROPHOTOMETER SCANS

(see Figure 4, 3, lower trace).

In comparison with the infra-red radiation reflected from a rough aluminium surface (100%), the Weatherguard finish re-radiated at most 3%, the Bufftex (coarse grained surface) 2% and the matt-white surface 7%. These comparisons were made at a wavelength of 2, 5 microns. The Weatherguard scan indicated no increase in reflectivity above the 3% level over the wavelength range 2, 5 to 10 microns. Whilst low infra-red reflectivity was desired from the parabola surface it was necessary to ensure that no signal attenuation occurred.

4. 4 Absorption of microwaves by paint surfaces

Measurements were taken of the absorption by the paint surfaces of microwaves at 22 GHz. A suitably attenuated Varian Gunn diode connected to a horn feed was used to transmit energy onto the paint samples. A Hewlett-Packard thermistor mount attached to a horn feed and connected to a power meter was used as a 22 GHz detector. The reflected energy detected was compared with a direct measurement at an equivalent distance. No attenuation greater than 0, 1 dB was measured. This result is in agreement with measurements made at the National Radio Astronomy Observatory in the United States (Hass, 1974), where the maximum absorption loss at 86 GHz due to "Triangle Hi-reflectance Flat White No. 6" was found to be 0, 06 dB.

The Weatherguard surface appeared to be more durable than the coarser grained Bufftex finish and was selected.

The main parabolic reflector was thus painted with two coats of Buffalo Calcium Plumbate Alkyd based primer, two coats of Buffalo Plykote Universal undercoat and finally two coats of Dulux Weatherguard brilliant white.

The final test was performed when the painted surface was directed at the Sun. The surface temperature of the sub-reflector remained at a satisfactory level.

The paint surface has not deteriorated over a period of six months.

CHAPTER FIVE

THE SOLAR SYSTEM AT 22 GHz

CHAPTER FIVE

THE SOLAR SYSTEM AT 22 GHz

The Sun, Moon, Venus and Jupiter are strong and accurately positioned radio sources that can be used as test transmitters for measurements of antennas. The Rhodes radio telescope is not particularly sensitive and the observation of elements of the solar system at 22 GHz can provide operational experience. A complete survey of the solar system near a wavelength of one centimetre is not available. This chapter hence reviews observations published prior to January 1975.

In the summary estimates of expected flux and integration times required are presented as well as suggestions for further study.

5. 1 The Sun

At microwave frequencies three forms of emission from the Sun are generally studied. These are, emission associated with the quiet Sun, the s or slowly varying component and emission associated with radio bursts.

The emission from the quiet Sun at 22 GHz is probably a stable radiation level produced by thermal bremsstrahlung in or near the chromosphere (Hjellming and Wade, 1971). Typical brightness temperatures observed are 11000 K at 22, 2 GHz (Staelin, 1968) and 9700 $\pm$ 600 at 22, 7 GHz (Efanov and Moiseev, 1971). Shimabukaro and Stacey (1968) review results for the quiet Sun at centimetre and millimetre wavelengths.

Hjellming and Wade (1971) associate the s-component with protrusions of denser plasma from the photosphere (temperature approximately 6000 K).

However the s-component peaks at about a wavelength of 10 centimetres (10^6 flux units) and hence this cannot be explained as simple thermal radiation. Hjellming and Wade (1971), Figure 1 shows that at 22 GHz the s-component is probably not detectable above the quiet Sun emission.

22 GHz is a useful frequency to use for the study of solar radio bursts. Croom and Powell (1971) have studied bursts over a period of several years at 19 GHz and have shown that the more intense bursts have their spectral peak in a frequency region above 10 GHz. They have detected fifteen bursts with flux greater than 10^7 flux units.

5.2 The Moon

The Moon behaves very much like a black body at 250 K however the brightness temperature varies with the phase of the Moon according to equation 5.1 (Piddington and Minnett, 1949).

$$T_F = T_{F=} - T_{F\sim} \cos(\psi - \psi_o) \qquad 5.1$$

where $T_{F=}$ is the mean effective temperature, the constant component, $T_{F\sim}$ is the amplitude of the variation in temperature, ψ is the lunar phase and ψ_o is the phase shift. Accurate measurements by Piddington and Minnett, Dmitrenko (1964) and Krotikov (1961) indicate that

$$T_{F=} = 215 \pm 10 \text{ K} \qquad \text{at} \quad 1,25 \text{ cm}$$
$$T_{F\sim} = 35 \text{ K} \quad \text{(no error given)}$$

These figures are in reasonable agreement with Moran (1966).

$$T_F = 217 \text{ K (no error given) at } 1,37 \text{ cm}$$
$$T_{F\sim} = 21 \pm 2 \text{ K}$$

However values for ψ_o are not in close agreement. Piddington and Minnet (1949) and Moran (1966) obtain $\psi_o = 45^\circ$ and 41° respectively which results in T_F reaching a peak some three and a half days after full Moon. Dmitrenko (1964) finds that at 1,65 centimetres ψ_o is between 8° and 18°.

The simple explanation for the phase retardation is that the solar heating reaches lower levels in the surface only after a certain delay associated with the thermal conductivity of the surface materials which is probably fairly low (Steinberg 1963, page 162, Troitskii 1967). Further support for this explanation comes from the absence of significant changes in microwave temperatures during an eclipse of the Moon.

By far the most detailed estimates of the mean brightness temperature at wavelengths between 10 μm and 100 cm have been made by Linsky (1973). He finds an estimated best value of 239,5 $\pm$ 10,1 K at 1 cm. Linsky considers surface types, soil samples and surface measurements made by Apollo teams.

5.3 Mercury

Observations of Mercury are difficult because the planet is of small angular size, subtending approximately 11 seconds of arc at mean conjunction. Furthermore the planet's angular distance from the Sun is never more than 28^{o}.

Most observers agree that Mercury is thermophysically similar to the Moon (Morrison and Klein 1970, Welch 1966) a conclusion supported by papers including Mariner 10 observations presented at a recent (April, 1974) meeting of the American Astronomical Society (Hartmann, 1974). However no agreement has been reached on phase variations. Welch (1966) claims that at shorter wavelengths a periodic variation with phase angle should be observed with the radio maximum brightness from a given point on the surface somewhat delayed behind the maximum surface temperature. Welch observed a brightness temperature of 450 $\pm$ 60K at 1,53 cm with the phase angle varying between 110^{o} and 138^{o}. Golovkov (1968) worked at 0,8 cm and finds the brightness temperature, T_b, to be given by,

$$T_b = 530 \pm 50 + (290 \pm 70) \cos (\Phi \pm 15^o) \text{ K} \qquad 5.2$$

where Φ is the phase angle.

Morrison and Klein (1970) observed a phase invariant component

$$T_b = 350 \pm 30 \text{ K} \quad , \quad \lambda = 1,95 \text{ cm}$$
$$= 385 \pm 20 \text{ K} \quad , \quad \lambda = 6,0 \text{ cm}$$

They study all known microwave measurements except observations by Welch and Golovkov which they ignore and find that the time averaged disk temperature of Mercury increases by 25% from short millimetre wavelengths to 6 centimetres wavelength.

The brightness temperature at 1, 35 cm interpreted from Figure 4 of Morrison and Klein (1970) is approximately 320 ± 50 K. The authors claim a departure from a thermal spectrum due to an increase in temperature with depth. They suggest that this temperature gradient could be maintained by a sub-surface "greenhouse effect" if radiative heat conduction, which is strongly temperature dependent, supports a large portion of the diurnal flow of heat in Mercury's epilith. They claim that their observations are consistent with a model in which the ratio of the electrical to thermal skin depths is near unity at a wavelength of 1 cm.

5.4 Venus

Venus has been thoroughly studied at microwave frequencies with little agreement on brightness temperature, phase variations or suitable models.

Brightness temperatures have been carefully measured over a number of wavelengths near the 1, 35 cm water vapour line. Results vary from 436 ± 39 K (Law, 1968) to 540 ± 20 K (Janssen 1972, Griffith 1967, Welch and Thornton 1965). Janssen (1972) suggests that the Law and Staelin measurements may be 20% low. He cites their result for the brightness temperature of Jupiter which is suspect (see Section 5.6).

A comparison by Barrett (1965) of observations made by Welch and Thornton (1965) and Staelin and Barrett (1965) suggests that the spectrum of Venus near 1 cm may be a function of time.

Prior to 1965 large phase variations were observed at several frequencies with differences in disk temperatures amounting to between 80 and 150 K. Gibson and Corbett (1965), for example, present their results at 1,35 cm as:

$$T_b = 430 - 440 \text{ K} \qquad \text{for } h < 0,19$$
$$T_b = 320 \pm h \times 600 \text{ K} \quad \text{for } 0,6 > h > 0,19 \quad (i < 130^{\circ})$$

where h is the fraction of the disk illuminated and i is the Sun-Venus-Earth angle. The authors put forward no explanation for the large brightness variation with phase.

More recent measurements, reviewed by Janssen (1972) show that the variations are at most 25 K (see Morrison, 1969 for example) and earlier measurements are considered in error.

Janssen suggests that large phase variations are unlikely as Venus's atmosphere has an enormous heat capacity. He shows that the average solar heat input during one Venus day (117 days) would raise the mean temperature only by about 2 K.

Ingersoll (1971) surveys many theories of the high surface temperatures on Venus. These differ as to how the surface is heated and how the heat is trapped near the surface. Trapping may be due to reflection of upward propagating radiation at the base of the cloud cover, absorption or absorption and reflection by dust in the lower atmosphere or absorption by atmospheric gases. In greenhouse models heat is deposited directly by sunlight either at the surface or in the lower atmosphere. In internal heating models, no solar heat is deposited but the infra-red opacity of the atmosphere is so great that planetary heat can maintain the high surface temperatures.

More recent models (Janssen 1972) are based on an atmosphere containing 95% CO_2, 5% N_2 and 0% H_2O. All observations near 1,35 cm show no indication of microwave resonances resulting from water vapour (Law and Staelin 1968, Welch 1965, Drake 1965, Janssen 1973a).

5.5 Mars

Janssen (1973b) has observed Mars at 22 GHz and finds a brightness temperature of 181 ± 11 K. He suggests that the emission is wavelength independent. Hobbs (1968) worked at 1,55 and 0,95 cm and observed

$$T_b = 172 \pm 35 \text{ K} \qquad 1{,}55 \text{ cm}$$

$$T_b = 171 \pm 37 \text{ K} \qquad 0{,}95 \text{ cm}$$

Sagan (1971) has reviewed the microwave observations and finds that T_b decreases from long to short wavelengths, rather than increasing as expected from the solution of a one dimensional equation of heat conduction. He presents a model with a thin near surface layer of a material with high dielectric constant and high millimetre wave absorption. A model with a layer of liquid water some tens of microns thick, localized in the top few millimetres of a Martian epilith with refractive index approximately 1,6 also fits the microwave spectrum and the infra-red and radar data as well.

Ingersoll and Leovy (1971) consider that the Martian atmosphere has only a small effect on temperatures at the ground. This is due to the small heat capacity of the atmosphere and also to the small optical thickness of the atmosphere at most visible and infra-red wavelengths.

5.6 Jupiter

Measurements of Jupiter's disk temperature near 1,35 cm are listed below with references.

Janssen (1973b)	136 ± 5 K	1,35 cm
Wrixon (1971)	139 ± 6 K	1,33 cm
Law (1968)	107 ± 12 K	1,35 cm

(Janssen (1972) suggests that the Law (1968) measurement may be 20% too low.)

The brightness temperature at short centimetre wavelengths is close to infra-red values and is approximately that expected for a black body at the appropriate distance from the Sun. It may be noted that Jupiter's non-thermal component of emission does not contribute significantly at wavelengths less than 3 cm (Gulkis 1973a). Detailed measurements of T_b in the vicinity of 1,25 cm (Law 1968, Wrixon 1971) show a slight dip, interpreted by Kellermann (1970), Dickel (1970) and Wrixon (1971) as being due to the opacity of a high altitude, cool, saturated layer of ammonia. Wrixon (1971) claims that the decrease in flux should amount to only 12%. Gulkis (1973b) unsuccessfully searched for narrow-band ammonia lines.

Poynter and Gulkis (1972) have constructed model atmospheres for Jupiter and Saturn with major constituents being He and H_2 with trace ammonia. Each model atmosphere is in hydrostatic equilibrium with the low troposphere region in convective equilibrium and with an isothermal stratospheric region.

Most models (Welch, 1966 for example) predict that the atmosphere is saturated with ammonia at all levels above the visible clouds.

5.7 Saturn

Kellermann (1970) and Gulkis (1973a) have reviewed observations of thermal emission from Saturn and a brightness temperature of about 140 K may be deduced for a wavelength of 1, 35 cm. This is greater than the temperature of a rotating black body heated only by solar radiation. Gulkis (1969) suggests a model where there is thermal emission by a deep atmosphere with a temperature gradient. Wrixon and Welch (1970) have measured Saturn 's spectrum near the 1. 25 cm inversion band of ammonia and find evidence for its presence.

Measurements are often not made with sufficient angular resolution to determine the effect of the rings on the measured temperature. According to Kellermann (1970) the rings of Saturn may effect the observed temperature in two ways:

1. The changing tilt of the rings with respect to the Sun will cause a variation in the total solar flux that reaches the disk of the planet.

2. The changing tilt of the rings with respect to the earth will cause a variation in the area of the disk obscuredby the rings.

NRAO observations at 2 cm appear to indicate a combination of both effects. However, accurate measurements are required to determine the opacity of the rings to the solar heating as well as the opacity at radio frequencies.

Cuzzi and van Blerkom (1974) put a lower limit of about 15 K on the brightness temperature of the rings at microwave frequencies.

5.8 Uranus, Neptune and Pluto

Observations of Uranus and Neptune are reviewed by Webster (1972). Brightness temperatures of 170 $\pm$ 20K (Uranus) and 165 $\pm$ 15K (Neptune) may be deduced for a wavelength of 1, 35 cm. The brightness temperatures are of the order of 100% greater than expected temperatures of respective black bodies heated by solar radiation.

Gulkis (1973a) and Kellermann (1970) suggest that T_b peaks at 2 cm and Pauliny-Toth (1970) working at 3, 5 , 9, 5 and 19, 5 mm finds a decrease in T_b with decreasing wavelength for both Uranus and Neptune.

Kellermann (1970) reports that an interesting variation in the solar heating occurs for Uranus which has its axis of rotation tilted by 98^{o} to the plane of the orbit. Twice during each revolution (once every 42 years) one pole is tilted toward the Sun and only a single hemisphere is heated. 21 years later the pole is pointed so that the rotation of the planet alternately heats each hemisphere every 10 hours, radiation is increased, and the temperature is reduced by $2^{\frac{1}{4}}$. The axis was last pointed towards the Sun in 1966 hence accurate measurements over some years may show up to a 20% drop in temperature.

Disk temperature calculations for Neptune made prior to 1968 may be 20% too great as a consequence of an under-estimation of angular size. Measurements by Taylor (1968) indicate that the diameter of Neptune may be 10% greater than that previously accepted.

Webster (1972) puts an upper limit for T_b of 167 K for Pluto. Pluto's blackbody equilibrium temperature is of the order of 45 K.

5.9 Summary and calculations of flux

The antenna temperature, T_A, due to a source is given by (Kraus, 1966, page 100)

$$T_A = \Omega_S \, T_b / \Omega_A \quad K \qquad 5.3$$

where Ω_S is the source solid angle, T_b is the average source brightness temperature and Ω_A is the antenna beam solid angle.

The observed flux density of a radio source is given by (Kraus, 1966, page 99)

$$S = 2\,k\,T_A / A_e \qquad \text{watts m}^{-2}\,\text{Hz}^{-1} \qquad 5.4$$

where k is Boltzmann's constant and A_e is the effective area of the dish.

$$\lambda^2 = A_e\,\Omega_A \qquad \text{(Kraus, page 157)} \qquad 5.5$$

where λ is the wavelength and therefore the observed flux is

$$\underline{S = 2\,k\,\Omega_S\;T_b/\lambda^2} \qquad \text{watts m}^{-2}\,\text{Hz}^{-1} \qquad 5.6$$

$$S = 4{,}61 \times 10^3\;\Omega_S\;T_b \qquad \text{flux units} \qquad 5.7$$

if the source solid angle, Ω_S, is given in deg.^{2} (A flux unit, f.u., is 10^{-26} watts m^{-2} Hz^{-1}.)

In Section 1.6 the minimum detectable temperature, ΔT_{min}, for a continuum source for our system is given as

$$T_{min} = (0{,}15 \pm 0{,}02)/(t\,n)^{\frac{1}{2}} \quad K$$

where t is the post detection integration time and n is the number of records. The minimum detectable flux is then

$$\underline{S_{min} = 2\,k\;\Delta T_{min}/A_e} \qquad W\,m^{-2}\,Hz^{-1} \qquad 5.8$$

$$S_{min} = (410 \pm 70)/t^{\frac{1}{2}} \qquad \text{f.u.} \qquad 5.9$$

if n = 1. The effective area of the dish, A_e, is 1,0 m^2 (see Section 6.3).

This is then the detectable flux in a given integration time, t, for a unity signal to noise ratio. Alternatively to observe a radio source of flux 410 f.u. with a signal to noise ratio of ten an integration time of 100 seconds is required.

A summary of observations is presented in Table 5.1. The expected flux at specified distances and the required integration times for a signal to noise ratio of ten have been calculated from equations 5.7 and 5.9 respectively. The source solid angles have been calculated from mean equatorial diameters given in Norton's Star Atlas, 1973, page 68. These figures are presented in Appendix D.

Table 5.1 indicates that only the Sun, Moon, Venus and Jupiter are detectable in reasonable integration times. However, the review of observations near a wavelength of one centimetre has indicated areas where further study might be worthwhile using our telescope. These are

a) the frequency and intensity of radio bursts from the Sun

b) the accurate determination of ψ_0, the phase shift in equation 5.1

c) the brightness temperature and phase variations of Venus.

Table 5.1

Summary of observations, calculations of expected flux at specified distances, estimation of required integration time, t, for a signal to noise ratio of ten.

Object	T_b(K)	Reference	λ (cm)	Flux expected at distance (f. u.)				
				min	mean	max	mean (time) inf. conj.	mean (time) oppn.
Sun	11000	Staelin 1968	1, 35		$1,15 \times 10^7$			
	9700 ± 600	Efanov 1971	1, 32		$1,02 \times 10^7$			
Moon	Max 251	Piddington 1949			$2,5 \times 10^5$			
		Dmitrenko 1964	1, 25					
	Min 179	Krotikov 1961			$1,8 \times 10^5$			
	Max 238				$2,4 \times 10^5$			
		Moran 1966	1, 37					
	Min 196				$2,0 \times 10^5$			
Mercury	320 ± 50	Morrison 1970	1, 35	15	3, 7	1, 8	12 (32 ± 12h)	
Venus	436 ± 39	Law 1968	1, 35	531	31	11	443 (86 ± 30s)	
	540 ± 20	Janssen 1972		660	39	14	549 (56 ± 19s)	
		Griffith 1967	1, 35					
		Thornton 1965						
Mars	181 ± 11	Janssen 1973b	1, 35	34	1, 9			16 (18 ± 6h)

Object	T_b(K)	Reference	λ (cm)	Flux expected at distance (f. u.)			
				min	mean	max	mean/oppn. (time)
Jupiter	136 ± 5	Janssen 1973b	1, 35	96	54	3, 5	84 (40 ± 14m)
	107 ± 12	Law 1968	1, 35	75	43	2, 8	66 (64 ± 22m)
Saturn	140	Kellermann 1970 Gulkis 1973a	1, 35	17	12	8, 8	15 (21 ± 7h)
Uranus	170 ± 20	Webster 1972	1, 35	0, 7	0, 5	0, 5	0, 6 (540 ± 200 days)
Neptune	165 ± 15			0, 3			
Pluto	< 167						

CHAPTER SIX

THE RADIO TELESCOPE - FIRST RESULTS

CHAPTER SIX

THE RADIO TELESCOPE - FIRST RESULTS

6.1 The detection of the Sun

Figure 6.1 is a pen recorder trace of the output of the continuum receiver integrator for a transit of the Sun through the main beam of the telescope. The spikes arise from pen recorder scale changes. The dotted lines depict the trace shape had the recorder been left on the more sensitive setting.

An estimate of the brightness temperature of the Sun was made by calibrating the continuum receiver RF detector output using the attenuated signal from the noise source as input. During calibration measurements the receiver input was switched between the fired noise tube and a matched load. During brightness temperature measurements on the Sun the receiver input was switched between the main horn and the unfired noise tube. The two front end arrangements for these measurements are shown in Figure 6.2. In each case the detector responds to power, W, given by

$$W = G\,k\,T\,B \qquad 6.1$$

where G is the amplifier gain, B is the bandwidth and k is Boltzmann's constant. For the calibration measurements the effective temperatures were

$$T_1 = T_R + T_0\,(1 - 1/L) + T_G/L \qquad \text{fired noise source}$$

and $$T_2 = T_R + T_0 \qquad \text{matched load}$$

For the Sun transit

$$T_3 = T_R + T_0 + T_{sky} + T_b \qquad \text{main horn}$$

$$T_4 = T_R + T_0 \qquad \text{unfired noise source}$$

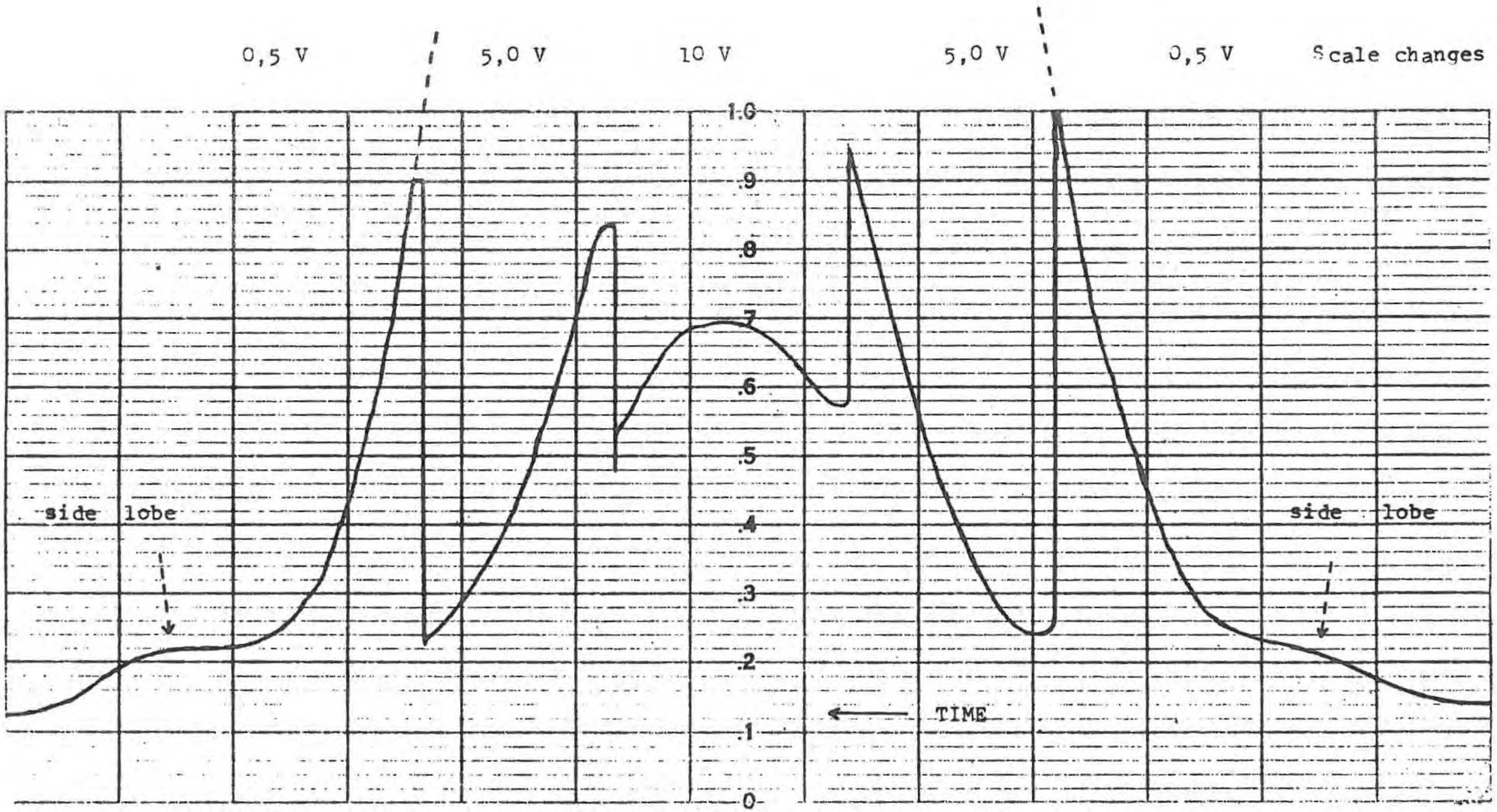

Chart speed 0,75"/min.

Receiver time constant 1s

FIGURE 6.1

OUTPUT CF THE CONTINUUM RECEIVER FOR

A TRANSIT OF THE SUN

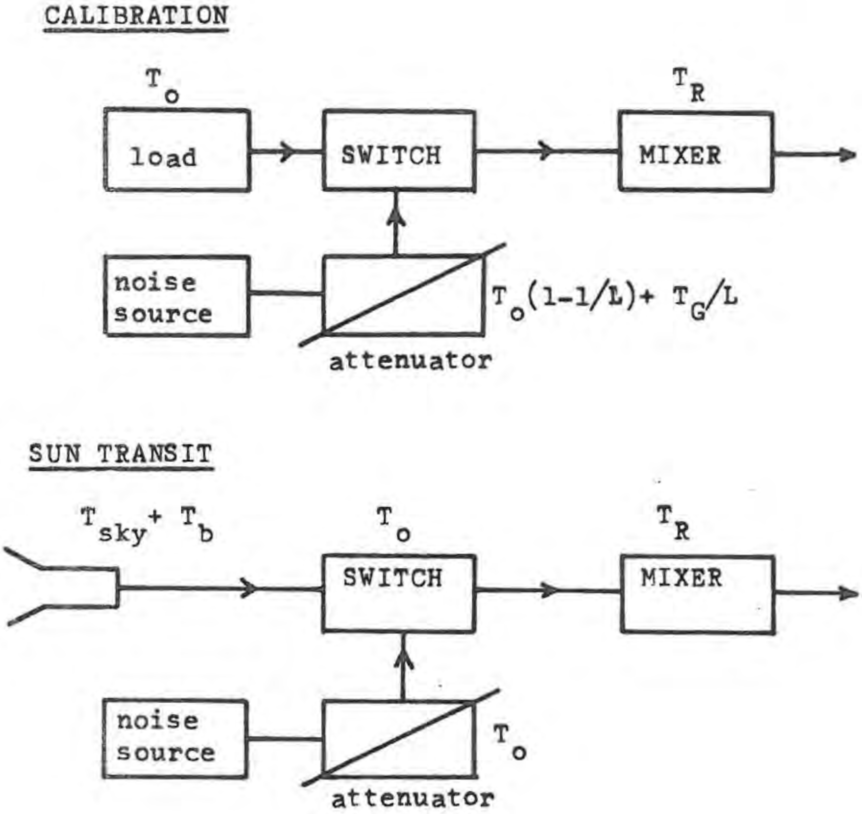

FIGURE 6.2

FRONT END ARRANGEMENT FOR SUN OBSERVATION

T_G = noise tube temperature (12 000 $\pm$ 400 K, see Section 1.1)

T_R = mixer noise temperature

T_0 = noise tube attenuator or matched load temperature

T_b = apparent source brightness temperature

T_{sky} = sky background temperature (about 50 K, see Section 1.6)

L = linear attenuation in the noise line

If T_1 and T_3 give equal detector outputs

$$T_{sky} + T_b = (T_G - T_0)/L \qquad 6.2$$

The attenuation in the switch and waveguide (0,4 dB) will affect both measurements equally. A calibration curve of detector output versus $(T_G - T_0)/L$ is shown in Figure 6.3. When the horn was pointed at the Sun the detector output was 220 mV.

Therefore, $T_{sky} + T_b = 2370 \pm 50$ K

and $T_b = 2320 \pm 50$ K

Baars (1973) has analysed the effect of the finite angular size of the source on the result and he presents a correction factor K such that for a disk source

$$K = x^2/(1 - \exp(-x^2)) \qquad 6.3$$

where

$x = R/(0,6\ \Theta_A)$

R = disk source angular radius

Θ_A = half power beam width (HPBW) of the telescope

For the Sun, $R = 0,268^o$.

The antenna beam has been measured using the test transmitter described in Section 2.10. The transmitter was placed 100 metres from the telescope at a point 10 metres above the ground. The telescope was moved in azimuth across the transmitter beam path. The detector output was measured for various azimuth positions. A source calibration curve similar to Figure 6.3 has been used. The antenna beam pattern is shown in Figure 6.4. The measured HPBW, Θ_A is $0,45 \pm 0,02^o$. Hence the Baars correction constant K is

$$K = 1,57 \pm 0,07$$

and the corrected value of T_b is then

$$T_b' = 3640 \pm 180 \text{ K}$$

FIGURE 6.3

CALIBRATION CURVE FOR THE MEASUREMENT OF THE BRIGHTNESS TEMPERATURE OF THE SUN

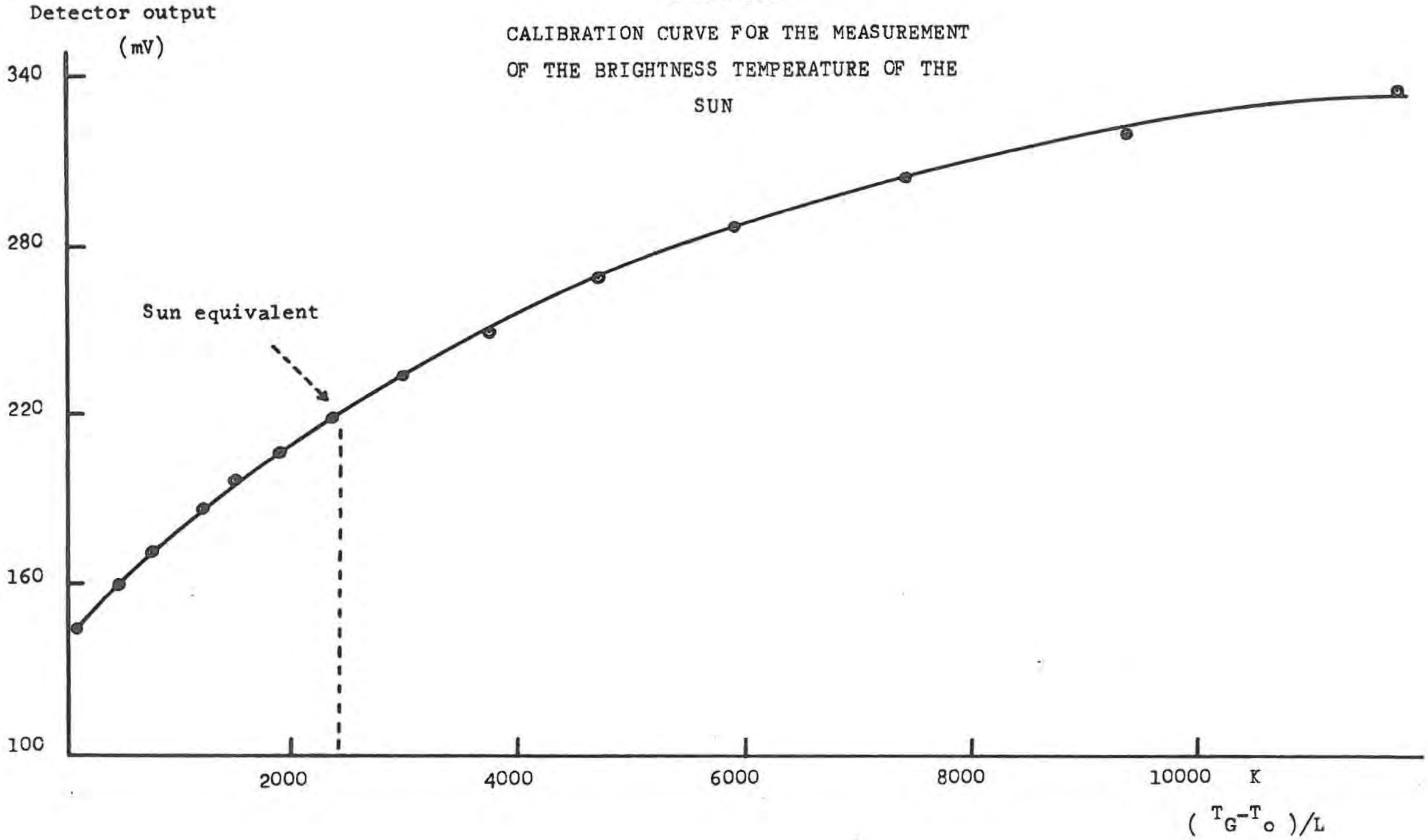

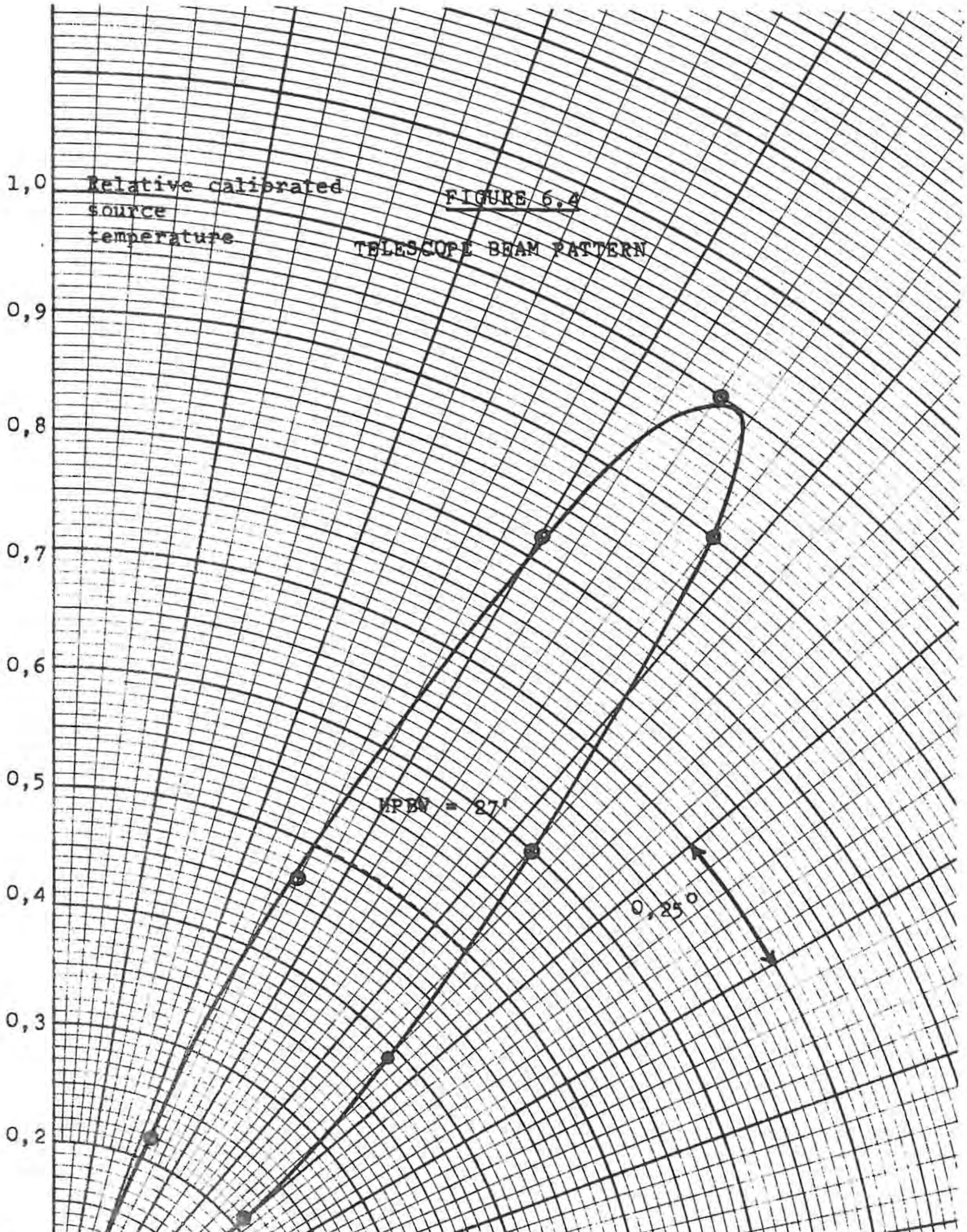

FIGURE 6.4

TELESCOPE BEAM PATTERN

Staelin (1966) and Davies (1973) have carried out extensive measurements of atmospheric absorption of microwaves at frequencies near 22 GHz. The zenith opacity for a clear day amounts to about 0,4 dB. The Sun measurements quoted were taken at 10.00 hours UT on the 15th November 1974 with an elevation angle of 75^o in clear sky. Davies (1973) indicates that the attenuation varies as the cosecant of the angle of elevation.

The value of T_b corrected for atmospheric absorption is then

$$\underline{T_b'' = 4100 \pm 200 \text{ K}}$$

Section 5.1 presents brightness temperatures of the Sun near 22 GHz measured by Staelin (1968), 11000 K, and Efanov (1971), 9700 $\pm$ 600 K. T_b'' is substantially less than these values because of the inefficiency of the feed horn and for reasons detailed in Section 6.4. The mean value is 10000 $\pm$ 1000 K and hence the aperture efficiency, ϵ_{ap}, of the telescope for this measurement is

$$\epsilon_{ap} = 0,41 \pm 0,05$$

6.2 The detection of the Moon

The signal from the Moon is much smaller than that from the Sun and therefore the receiver integrator output was used instead of the detector output. A pen recorder trace of the output of the continuum receiver integrator for a transit of the Moon through the telescope main beam at 17.20 hours U.T. on the 22nd April 1975 is shown in Figure 6.5. Adjacent to this record is an equivalent output when the noise generator attenuated by 24,6 $\pm$ 0,1 dB was fired for 30 seconds.

Once again equation 6.1 holds but a conventional front end arrangement was used for the specified Moon observation and the receiver input was simply switched between the main and secondary horns. The system is

Noise fired for 30s

Attenuation 24,6 ± 0,1 dB

0,5 V Scale

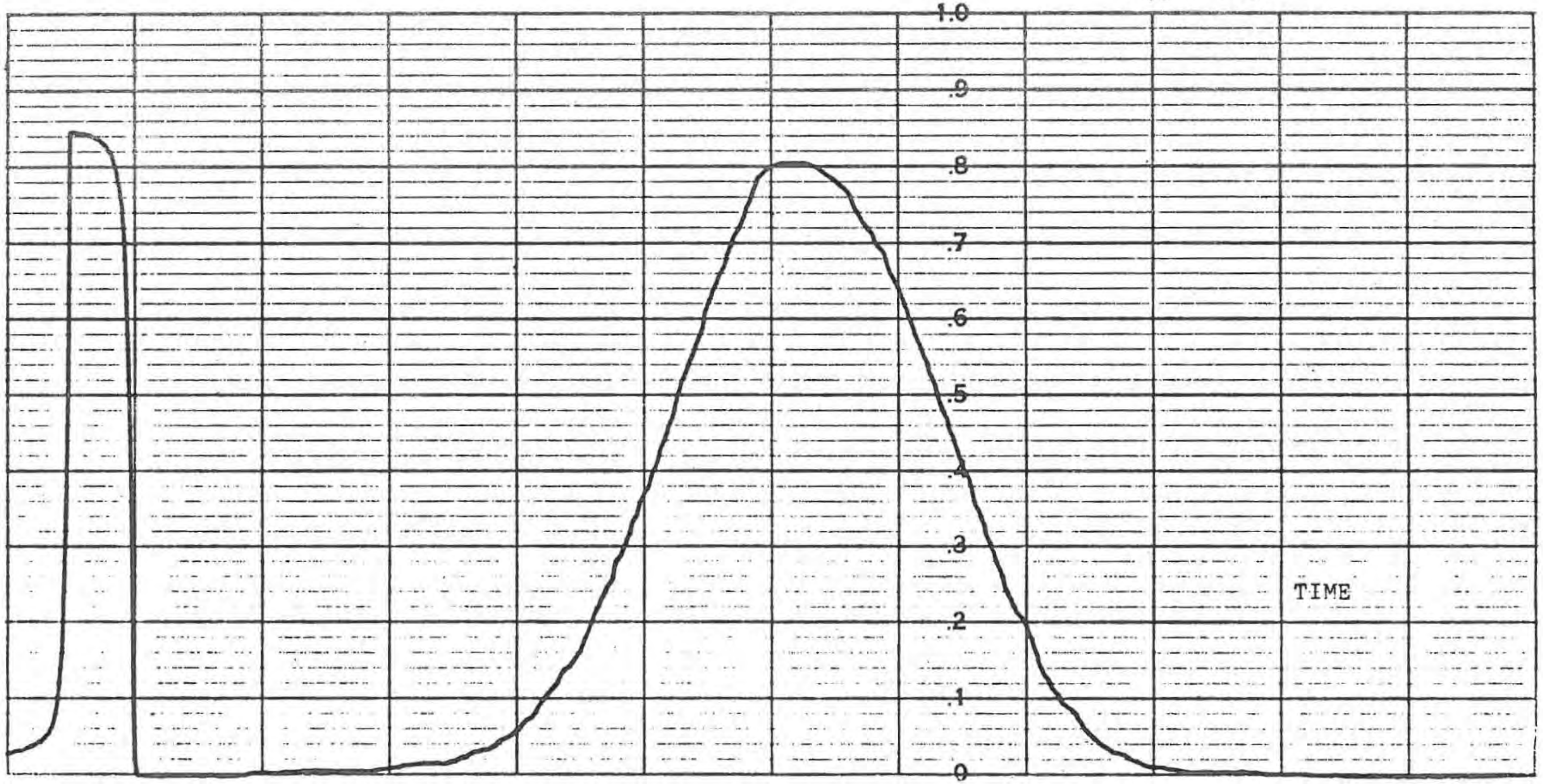

Chart speed 0,75"/min.

Receiver time constant 3s

FIGURE 6.5

OUTPUT OF THE CONTINUUM RECEIVER FOR A TRANSIT

OF THE MOON COMPARED WITH EQUIVALENT NOISE SOURCE illustrated in Figure 6.6.

In this case for the Moon transit

$$T = T_R + T_0 + T_{sky} + T_b \qquad \text{main horn}$$

$$\text{vs} \qquad T_R + T_0 + T_{sky} \qquad \text{secondary horn}$$

and for the fired noise generator

$$T = T_R + T_0 (1 - 1/L) + T_G/L + T_{sky}$$

$$\text{vs} \qquad T_R + T_0 + T_{sky}$$

Hence

$$T_b = (1/L)(T_G - T_0)$$

$$= 40 \pm 1 \text{ K}$$

Once again the Baars correction factor K can be applied using a Moon angular radius of $0,259^{\circ}$ and a HPBW of $0,45 \pm 0,02^{\circ}$ as before.

$$K = 1,53 \pm 0,07$$

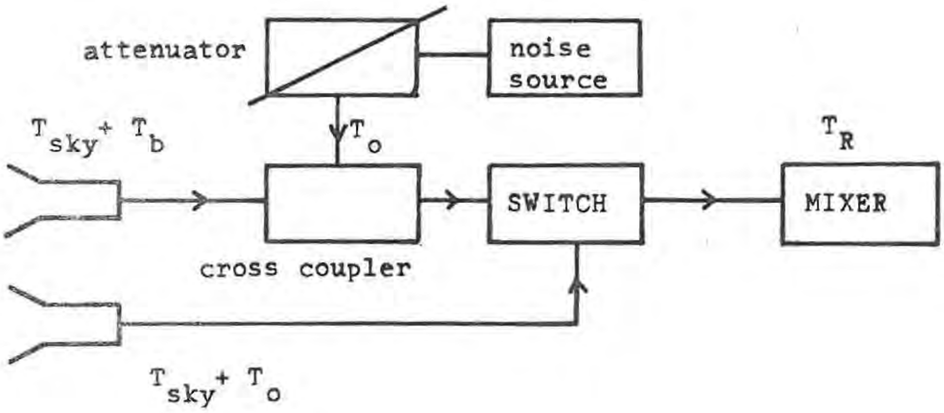

FIGURE 6.6

FRONT END ARRANGEMENT FOR MOON OBSERVATION

The correction factor for atmospheric attenuation can be calculated from the Moon elevation angle of $56,6^{\circ}$ at the time of observation. The clear sky attenuation figure of 0,4 dB is again used.

The final corrected T_b is

$$\underline{T_b'' = 80 \pm 4 \text{ K}}$$

Measurements of the Moon brightness temperature near frequencies of 22 GHz were considered in Section 5.2. Equation 5.1 was used to correct for phase effects. The Moon observation was made three days prior to full moon and therefore a temperature of 219 ± 10 K was calculated.

Hence the aperture efficiency for this observation was

$$\epsilon_{ap} = 0,37 \pm 0,03$$

6.3 Mean aperture efficiency, effective area and beam efficiency

The mean aperture efficiency from the two results is

$$\epsilon_{ap} = 0,39 \pm 0,04$$

and the effective area is

$$A_e = \epsilon_{ap} A_p$$

where A_p is the physical area of the dish, $2,63 \text{ m}^2$.

$$A_e = 1,0 \pm 0,1 \text{ m}^2$$

The beam efficiency

$$\epsilon_M = \epsilon_{ap} A_p \Omega_M / \lambda^2$$

where Ω_M is the main beam solid angle

$$\Omega_M = \theta_A^{\ 2}$$

Hence $$\epsilon_M = 0,35 \pm 0,04$$

6.4 Possible causes of inefficiency

Efficiencies of about 50% are typically obtained for the type of antenna and feed horn being used. Baars (1975) has studied the measurements and calculations presented in this Chapter and has suggested further causes of telescope inefficiency. In order of importance these are:

a) Large scale variations in the parabolic shape.

Gaylard (1975) has shown that the parabola is distorted. The scale of the variations is presently being analysed.

b) The effect of subreflector axial defocussing.

This has been measured (with Gaylard) using the Sun as a test transmitter. The reflector was placed in an optimum position before the above results were obtained.

c) Lateral defocussing of the subreflector.

Figure 6.1 illustrates an asymmetrical sidelobe structure. This indicates lateral defocussing and/or parabolic variations.

d) Beam separation.

Baars (1975) has calculated a beam separation of 1, 1 HPBW in elevation for the main and secondary horns. The separation, he suggests, should be two or three times this as in Sun and Moon observations the extended source fills parts of both beams and a signal loss occurs. Gaylard has shown that the loss is approximately 10%. This is confirmed in this Chapter. The aperture efficiency for the Sun measurements where only one horn was used (see Figure 6.2) is just 10% higher than the efficiency in the case of Moon observations where the conventional beam switching method was used (see Figure 6.6).

e) Subreflector parameters.

The subreflector has been checked by Gaylard and the surface is correct to 0, 1 mm. The aperture illumination is not optimum but Baars feels this is of secondary importance.

CHAPTER SEVEN

CONCLUSION

An analysis of the 22 GHz front end has been presented in Chapter One. Measurements of the noise temperature of the 22 GHz mixer have enabled estimates of the minimum detectable temperature to be made. The mixer temperature is in agreement with specifications. A successful method of frequency switching the front end local oscillator has been developed.

The spectral line and continuum receivers have been designed. Twenty line channels have been built and tested. They have been shown to operate as required. The continuum receiver has been constructed and used to detect the Sun and Moon at 22 GHz. Antenna alignment and testing has been undertaken. The spectral line receiver cannot be used for the detection of water vapour sources until the antenna servo and automatic control units have been completed because of the long integration times required.

Details of the receiver and logic power supplies are given in Appendix B4 and Chapter Two. Chapter Three presents the principles involved in tracking a radio source. A computer programme has been developed for this purpose.

A suitable paint surface for the parabolic reflector has been tested and used. This surface prevents excessive heating of the hyperbolic subreflector.

A literature survey of emission near a wavelength of one centimetre from the solar system has been undertaken. The Sun, Moon, Venus and Jupiter are well defined sources and are suitable test transmitters for antenna measurements. The expected flux and required integration times have been calculated.

Finally estimates of the efficiency of the telescope have been made from the observation of the Sun and Moon. Details are given of sources of inefficiency.

With the construction of the telescope drive and feedback units and the installation of the remaining spectral line channels the Rhodes 22 GHz radio telescope, as initially envisaged, will be complete. Full tracking facilities will enable integration times to be increased by a factor of one hundred.

LITERATURE CITED

Araki, T and M. Hirayama (1971). "A 20 GHz integrated balanced mixer," IEEE Trans. Microwave Theory Tech. MTT-19, 638.

The Astronomical Ephemeris for the year 1973. Her Majesty's Stationery Office, London (1971).

——————————— 1975. H.M.S.O., London (1973).

Baars, Jacob W.M. (1973). "The measurement of large antennas with cosmic radio sources," IEEE Trans. Antennas Propagat. AP-21, 461.

——————— (1975). Private communication.

Baart, E.E. (1973). Private communication.

Barrett, A.H. (1965). "Passive radio observations of Mercury, Venus, Mars, Saturn and Uranus," J. Res. N.B.S. Radio Science 69D, 1565.

Cheung, A.C. et al. (1969). "Detection of water in interstellar regions by its microwave radiation," Nature 221, 626.

Collin, R.E. (1966). Foundations for Microwave Engineering. McGraw-Hill, New York.

Croom, D.L. and R.J. Powell (1971). "19 GHz (1,58 cm) solar radio bursts in the period July 1967 to December 1969," Solar Phys. 20, 136.

Cuzzi, Jeoffrey N. and David van Blerkom (1974). "Microwave brightness of Saturn's rings," Icarus 22, 149.

Davies, P.G. (1973). "Slant path attenuation at frequencies above 10 GHz," in Propagation of radio waves at frequencies above 10 GHz. The Institution of Electrical Engineers, London.

de Jager, G. (1975). Private communication.

Dickel, John R. et al. (1970). "The microwave spectrum of Jupiter," Radio Science 5, 517.

Dmitrenko, D.A. et al. (1964). Izv. Vusov, Radiofiz 7, No. 3.

Drake, F.D. (1965). "A search for 1,36 cm water vapour line in Venus," J. Res. N.B.S. Radio Science 69D, 1577.

Efanov, V.A. and I.G. Moiseev (1971). "Observations of the solar radio emission at 8, 13 and 16 mm," Izv. Krymskoj Astrofiz. Obs. 43, 21.

Elder, H.E. and V.J. Glinski (1969). "Detector and mixer diodes and circuits," in Microwave Semiconductor Devices and Their Circuit Applications. Ed. H.A. Watson. McGraw-Hill, New York.

Explanatory Supplement to the Astronomical Ephemeris. H.M.S.O. London (1961).

Gardner, F.M. (1966). Phaselock Techniques. John Wiley, New York.

Gaylard, M. (1975). Private communication.

Gibson, J.E. and H.H. Corbett (1965). "Radiation of Venus at the 13,5 mm water vapour line," J. Res. N.B.S. Radio Science 69D, 1577.

Golovkov, V.K. and B. Ya. Lasovsky (1968). "Measurements of the phase dependence of the 0,8 cm radio emission of Mercury and some properties of its surface layer," Soviet Astr. -AJ 12, 299.

Griffith, P.H. et al. (1967). "The microwave spectrum of Venus in the frequency range 18-36 GHz," Icarus 6, 175.

Gulkis, S. et al. (1969). "The microwave spectrum of Saturn," Icarus 10, 421.

Gulkis, S. (1973a). "Thermal emission from the major planets," Space Sci. Rev. 14, 497.

Gulkis, S. et al. (1973b). "A search for narrow-band ammonia lines in the Jovian microwave spectrum," Bull. Am. Astron. Soc. 5, 287.

Hartmann, William K. (1974). "A 1974 tour of the planets," Sky and Telescope 48, 78.

Hass, Robert W. (1974). "RF absorption due to paint on the 36 foot antenna surface," NRAO Electronics Division Internal Report No. 140.

Helszajn, J. (1969). Principles of Microwave Ferrite Engineering. Wiley Interscience, London.

Hjellming, R.M. and C.M. Wade (1971). "Radio stars," Science 173, 1087.

Hobbs, R.W. et al. (1968). "Measurements of Mars at 1,55 cm and 0,95 cm wavelengths," Icarus 9, 360.

Ingersoll, A. P. and C.B. Leovy (1971). "The atmospheres of Mars and Venus," Ann. Rev. Astron. Ap. 9, 147.

Janssen, M.A. (1972). The 20-36 GHz Venus microwave emission. Space Sciences Lab., University of California, Berkeley.

Janssen, M.A. et. al. (1973a). "Venus: new microwave measurements show no atmospheric water vapour," Science 179, 994.

Janssen, M.A. and W.J. Welch (1973b). "Mars and Jupiter: radio emission at 1,35 cm," Icarus 18, 502.

Johnston, K.J. et al. (1972). "Microwave celestial water-vapour sources," Sky and Telescope 44, 88.

Kellermann, K.I. (1970). "Thermal radio emission from the major planets," Radio Science 5, 487.

Kraus, John D. (1966). Radio Astronomy. McGraw-Hill, New York.

Krotikov, V.D. et al. (1961). Izv. Vusov, Radiofiz 4, 759 and 1004.

Law, S.E. and D.H. Staelin (1968). "Measurement of Venus and Jupiter near 1 cm wavelength," Astrophys. J. 154, 1077.

Linsky, J.L. (1973). "The Moon as a proposed standard for microwave and infrared observations of extended sources," Astrophys. J. Suppl. 25, 163.

Microwave Engineers Handbook Volume 2 (1971). Compiled and edited by Theodore S. Saad. Artech House, Dedham, Massachusetts.

Moran, J.M. and D.H. Staelin (1966). "Observations of the Moon near 1 cm wavelength," Astron. J. 71, 865.

Morrison, David (1969). "Venus: Absence of a phase effect at a 2 cm wavelength," Science 163, 815.

Morrison, David and Michael J. Klein (1970). "The microwave spectrum of Mercury," Astrophys. J. 160, 325.

Mountfort, P.I. (1975). Private communication.

Nicholson, P.S. (1974). "A phase-lock system at 100 GHz incorporating a facility for frequency switching," Journal of Physics E 7, 506.

Norton, Arthur P. (1973). Norton's Star Atlas. 16th ed., edited by G. E. Satterthwaite. Gall and Inglis, Edinburgh.

Pauliny-Toth, I. I. K. and K. I. Kellermann (1970). "Millimetre-wavelength measurements of Uranus and Neptune," Astrophys. Lett. 6, 185.

Piddington, J. H. and H. C. Minnett (1949). "Microwave thermal radiation from the Moon," Austral. J. Sci. Res. 2, 63.

Poynter, R. and S. Gulkis (1972). "Thermal radio emission from Jupiter and Saturn," Bull. Am. Astron. Soc. 4, 361.

Sagan, C. and J. Veverka (1971). "The microwave spectrum of Mars: An analysis," Icarus 14, 222.

Shimabukaro, F. I. and J. M. Stacey (1968). "Brightness temperature of the quiet Sun at centimetre and millimetre wavelengths," Astrophys. J. 152, 777.

Staelin, D. H. and A. H. Barrett (1965). "Radio measurements of Venus near 1 cm wavelength," Astron. J. 70, 330.

Staelin, David H. (1966). "Measurements and interpretation of the microwave spectrum of the terrestial atmosphere near 1 centimetre wavelength," J. Geophys. Res. 71, 2875.

Staelin, D. H. et al. (1968). "Spectrum measurements of the Sun near 1 cm wavelength," Solar Phys. 3, 26.

The Star Almanac for Land Surveyors for the year 1973. H. M. S. O. London (1972).

Steinberg, J. L. and J. Lequeux (1963). Radio Astronomy. Trans. by B.N. Bracewell. McGraw-Hill, New York.

Taylor, G.E. (1968). "New determination of the diameter of Neptune," Nature 219, 474.

Troitskii, V.S. (1967). "Investigation of the surfaces of the moon and planets by means of thermal radiation," Proc. Roy. Soc. A 296, 366.

Way-Jones, C. (1975). Private communication.

Webster, W.J. et al. (1972). "Interferometric observations of Uranus, Neptune and Pluto at wavelengths of 11, 1 and 3, 7 cm," Astrophys. J. 174, 679.

Welch, W.J. (1965). "Observations of the 1, 35 cm water vapour line in Venus," J. Res. N.B.S. Radio Science 69D 1580.

Welch, W.J. and D.D. Thornton (1965). "Recent planetary observations at wavelengths near 1 cm," Astron. J. 70, 149.

Welch, W.J., D.D. Thornton and R. Lohman (1966). "Observations of Jupiter, Saturn and Mercury at 1, 53 cm," Astrophys. J. 146, 799.

Wrixon, G.T. and W.J. Welch (1970). "The millimeter wave spectrum of Saturn," Icarus 13, 163.

Wrixon, G.T., W.J. Welch and D.D. Thornton (1971). "The spectrum of Jupiter at millimeter wavelengths," Astrophys. J. 169, 171.

APPENDICES

APPENDIX A1

Major Front End Components

Component	Manufacturer	Specifications
Mixer	Aerojet General Corporation	K-band balanced mixer and IF amplifier, 20-24 GHz, double channel noise 4, 3 to 6, 5 dB. L. O. power max 2 mW. Amplifier 10-110 MHz, >35 dB.
Switch	Electromagnetic Sciences Inc.	Ferrite switch, insertion loss < 0, 3 dB, isolation >20 dB.
Gunns	1) and 2) Varian	Varactor-tuned Gunn effect oscillators, operating temp <85^{o}C.
	Type L:	22, 180 to 22, 310 GHz ,60 to 64 mW Varactor tuning 2 < V < 30 Vdc Operating voltage 6, 2 V
	Type S:	22, 195 to 22, 325 GHz ,52-56 mW Varactor tuning 1 < V < 36 Vdc Operating voltage 5, 9 V
	3) Mid-Century Microwavegear	18-24, 4 GHz , 34-164 mW (measured)

Noise source

a) mount	Mid-Century Microwavegear	ENR 15, 9 - 16,2 dB
b) tube	English Electric Valve	Tube BS 386
c) power supply	Mid-Century Microwavegear	Type EE/7A, starting spike 3, 1 kV tube running voltage range 65-165 Vdc

Lock box	Sage Laboratories	Model 251 B
		RF input -30 to 0 dBm
		Lock range $\pm$ 30V
		Short term stability 1 in 10^8/sec
		Long term stability 1 in 10^7/day

APPENDIX A2

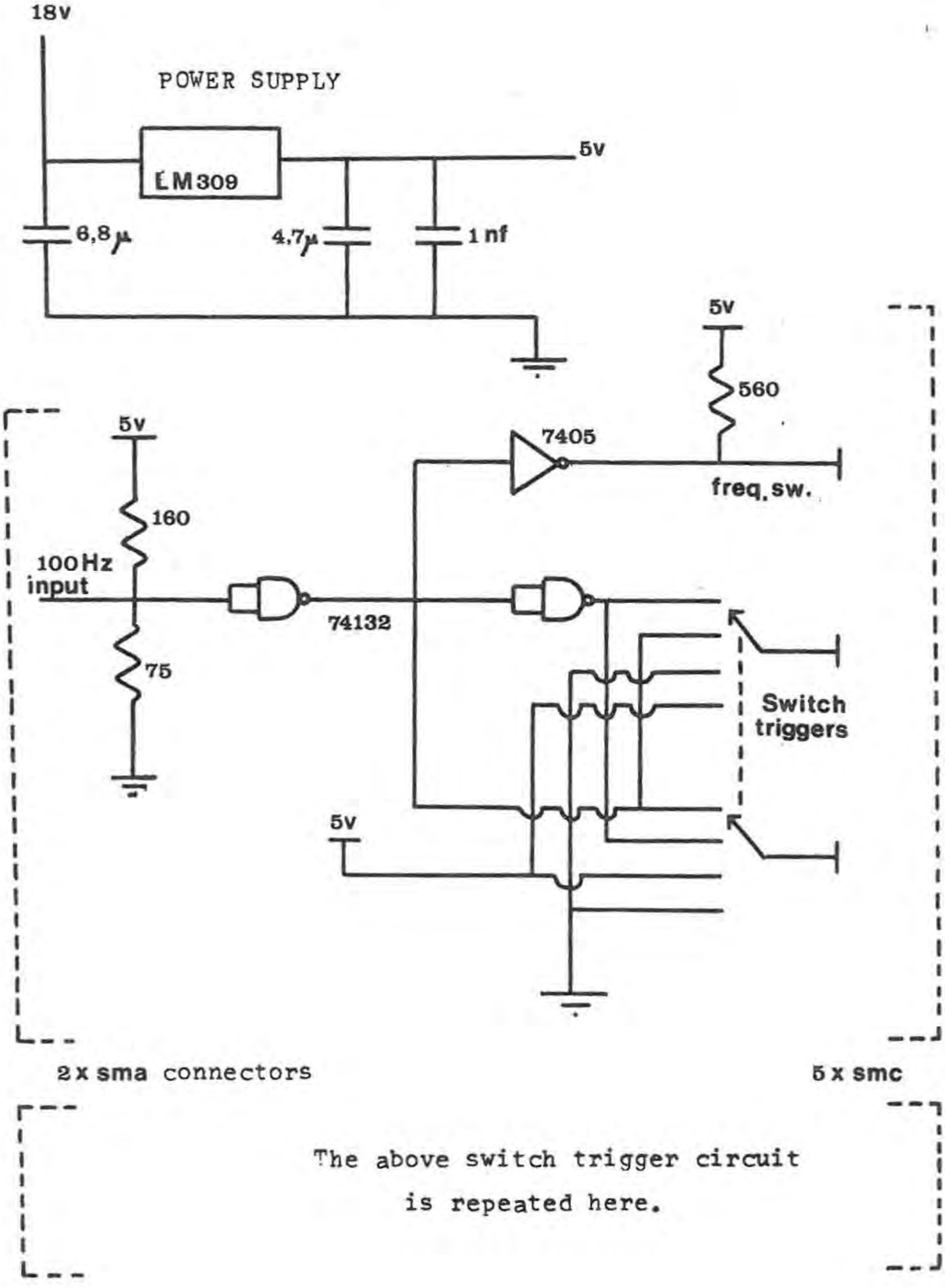

MICROWAVE SWITCH CONTROL

FREQUENCY SWITCH SIGNAL BUFFER

APPENDIX B1

RHG narrow band 30 MHz IF amplifier

Manufacturer's specifications

Centre frequency	30 MHz
3 dB bandwidth	10, 5 MHz
Maximum power gain	80 dB

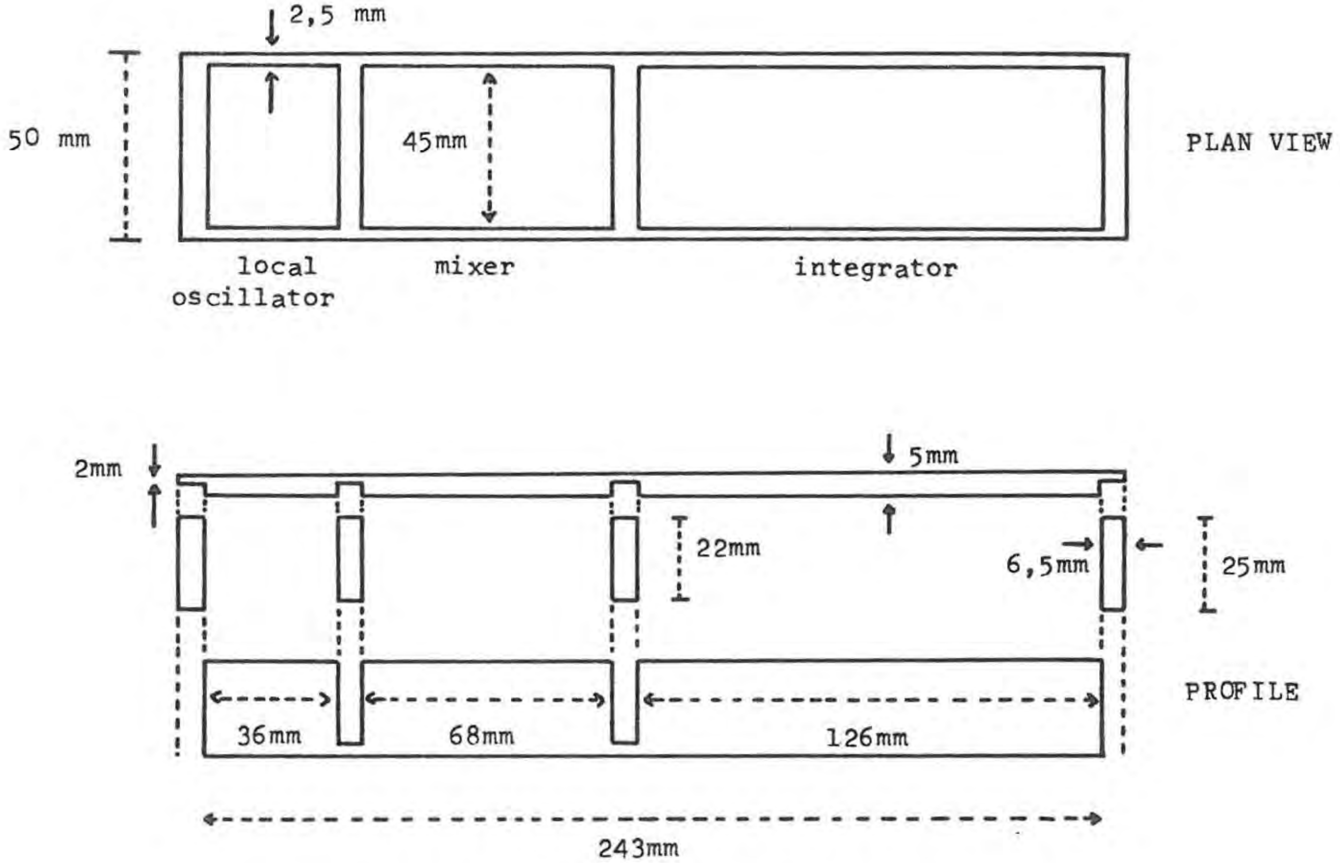

APPENDIX B2

Line receiver box design

Scale 1 : 2

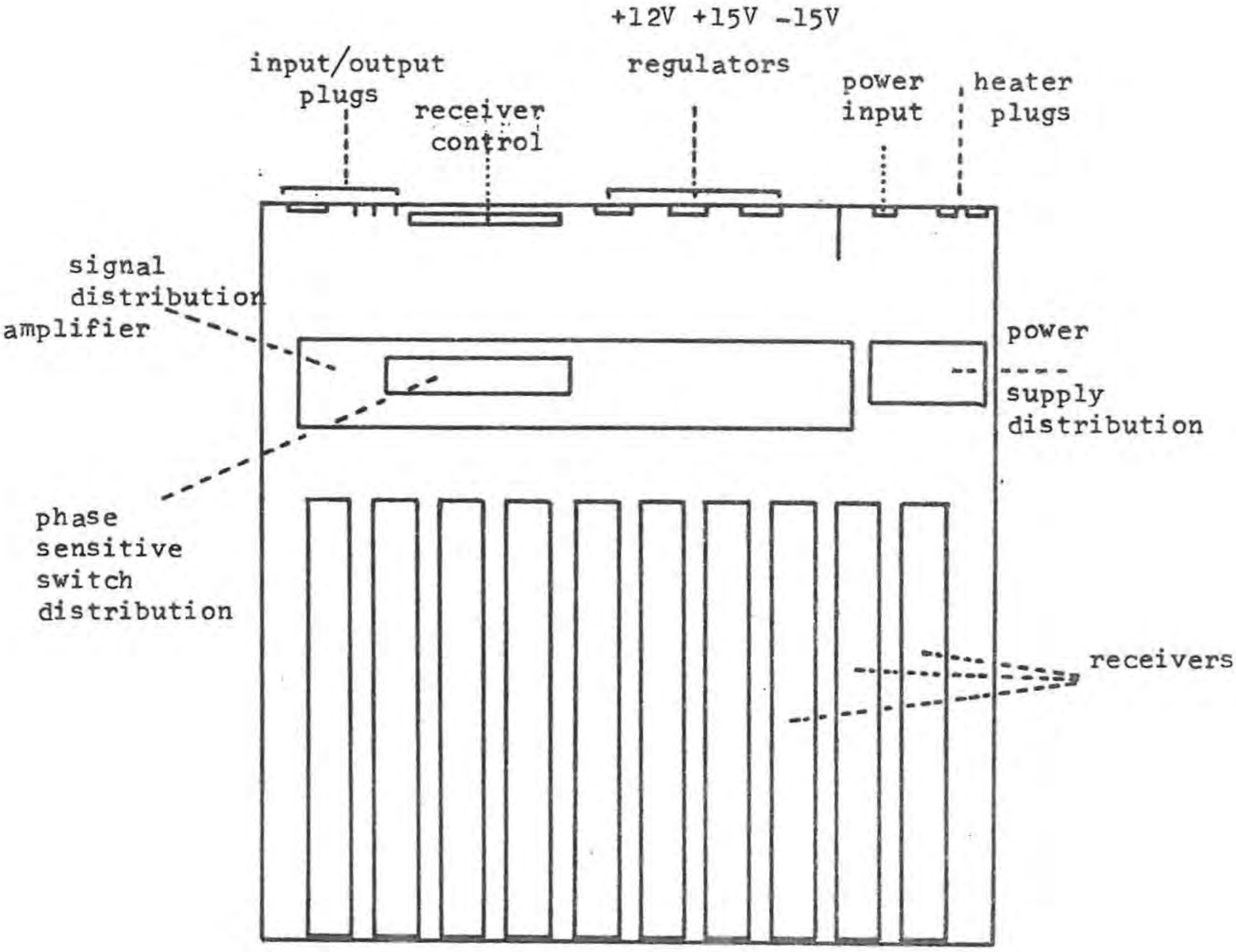

APPENDIX B3

Line receiver tray layout

APPENDIX B4

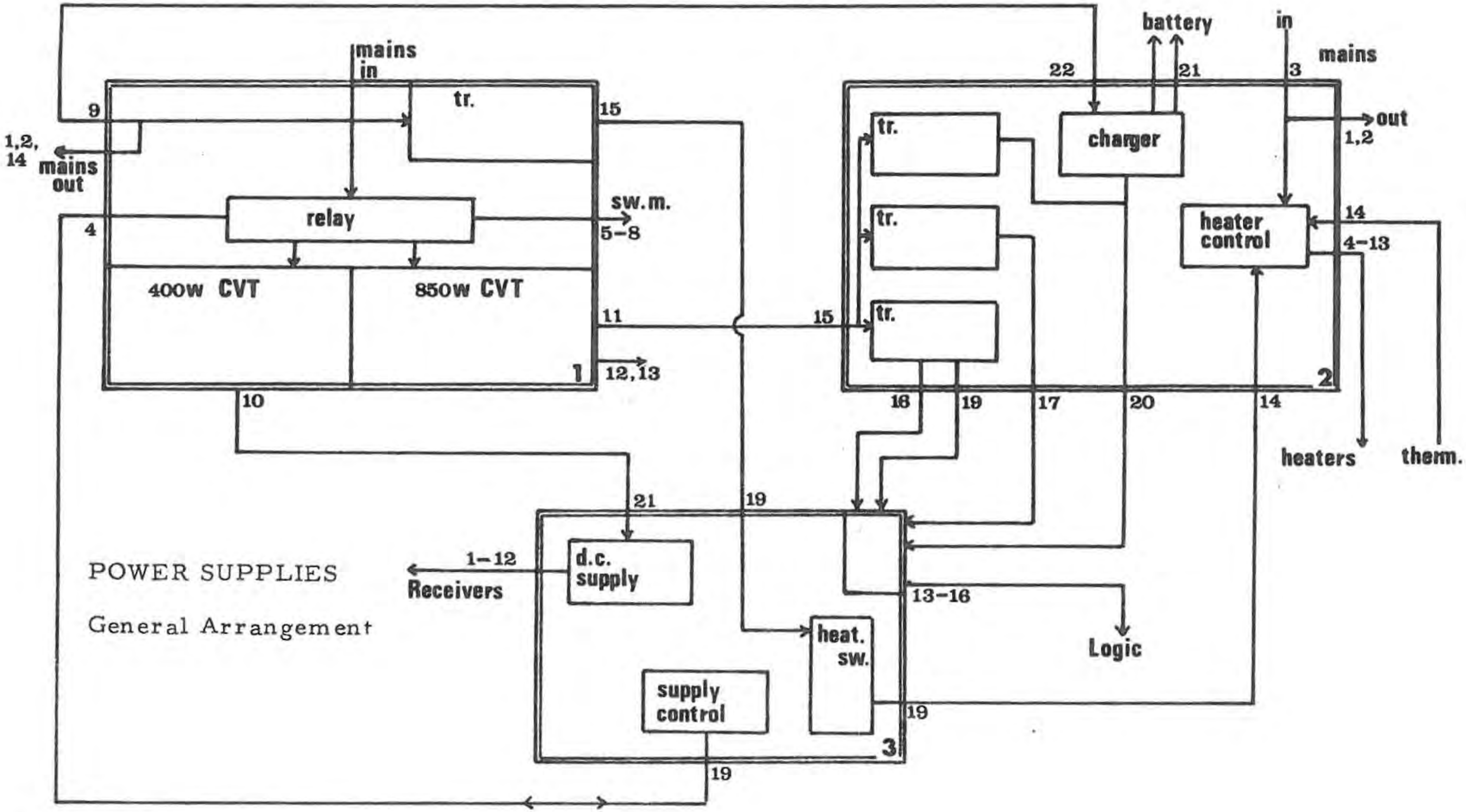

POWER SUPPLIES

General Arrangement

APPENDIX C

Source tracking programme H. P. Model 10, stored on magnetic card.

Data input to storage locations:

data	locations
α (1950) dec. deg	a
δ (1950) dec. deg	b
n_1 (1950) 1, 33617	007
N ($\rightarrow$ 1975) 25	008
n_2 (1975) 1, 33603	011
m_2 (1975) 3, 07374	013
m_1 (1950) 3, 07327	012
A	000
B	001
C Besselian day numbers	002
D	003
Greenwich apparent sidereal time 0^h U. T. dec. hours	014
Start of observation U. T. dec. hours	015
Increment dec. hours	020
End of run U. T. dec. hours	021

The maths and printer ROMS are required. The programme is entered at 000.

Subroutine	1 halts at	237	
	2	462	
	3 & 4	719	
	5	793	end.

The subroutines may be run separately. The most accurate α, δ always appear in a and b. For example for U. T. transit only:

Data input to storage locations:

data	locations
α	a
δ	b
G. A. S. T. 0^h U. T.	014

Instruction to H. P. model 10

GO TO 719

CONTINUE

APPENDIX D

Angular Equatorial Diameter

	Distance Min	Mean	Max	Mean Inf. Conj.	Mean Oppn.
Mercury	12, 9''	6, 4''	4, 5''	11, 37''	
Venus	66, 0	16, 0	9, 6	60, 32	
Mars	25, 7	6, 1	3, 5		17, 87''
Jupiter	50, 1	37, 9	30, 4		46, 86
Saturn	20, 9	17, 3	15, 0		19, 27
Uranus	3, 7	3, 3	3, 1		3, 20
Neptune	2, 2	2, 1	2, 0		2, 20
Pluto					0, 21

Solid Angle (deg^2)

	Distance Min	Mean	Max	Mean Inf. Conj.	Mean Oppn.
Sun		0, 22			
Moon		0, 21			
Mercury	$1, 01 \times 10^{-5}$	$2, 48 \times 10^{-6}$	$1, 23 \times 10^{-6}$	$7, 83 \times 10^{-6}$	
Venus	$2, 64 \times 10^{-4}$	$1, 55 \times 10^{-5}$	$5, 59 \times 10^{-6}$	$2, 20 \times 10^{-4}$	
Mars	$4, 00 \times 10^{-5}$	$2, 26 \times 10^{-6}$	$7, 42 \times 10^{-7}$		$1, 94 \times 10^{-5}$
Jupiter	$1, 52 \times 10^{-4}$	$8, 70 \times 10^{-5}$	$5, 60 \times 10^{-6}$		$1, 33 \times 10^{-4}$
Saturn	$2, 65 \times 10^{-5}$	$1, 81 \times 10^{-5}$	$1, 36 \times 10^{-5}$		$2, 25 \times 10^{-5}$
Uranus	$8, 30 \times 10^{-7}$	$6, 60 \times 10^{-7}$	$5, 82 \times 10^{-7}$		$7, 72 \times 10^{-7}$
Neptune	$2, 93 \times 10^{-7}$	$2, 67 \times 10^{-7}$	$2, 42 \times 10^{-7}$		$2, 93 \times 10^{-7}$
Pluto					$2, 67 \times 10^{-9}$